Supporting Information

Single-Molecule Graphene Quantum Dot: a Novel Efficient Photosensitizer for Photodynamic Cancer Therapy

Jintao Chen,[a] Shiru Yin,[a] Futing Yang,[a] Shengnan Guo,[a] Jiaojiao Zhang,[a] Zhenming Lu[a] and Tian Gao*[a]

[a] J. Chen, S. Yin, F. Yang, S. Guo, J. Zhang, Prof. Dr. Z. Lu, Prof. Dr. T. Gao
Interdisciplinary Institute of NMR and Molecular Sciences, Key Laboratory of Hubei Province for Coal Conversion and New Carbon Materials, School of Chemistry and Chemical Engineering, Institute of Advanced Materials and Nanotechnology, Wuhan University of Science and Technology, Wuhan 430081, China
E-mail: gaotian@whu.edu.cn

Table of contents

General information

All the chemicals and solvents were obtained from Bide Pharm and Sigma Aldrich and are of analytic grade purity and used without further purification. DI water is obtained through an intelligent ultra-pure water production system (Percolation Source, China). Silica gel (200-300 mesh & 0.040-0.063 mm) was packed for column chromatography. The products were characterized by ^{1}H NMR spectroscopy, ^{13}C NMR spectroscopy, and mass spectrometry. Nuclear magnetic resonance (NMR) spectroscopy was obtained with an Agilent DD2 600 spectrometer (600 MHz, ^{1}H NMR; 150 MHz, ^{13}C NMR) at 298 K in the indicated solvents of $CDCl_3$ (δ 7.26 and 77.16). Chemical shifts are expressed in ppm units concerning tetramethylsilane (TMS, 0.00 ppm, 1H). The following are abbreviations for multiples; s, singlet; d, doublet; t, triplet; q, quadruplet; dd, doublet of doublets; m, multiplet. All reactions were reacted in the atmosphere unless otherwise stated and were monitored for reaction progress using analytical thin-layer chromatography (TLC). Visualization was achieved by UV light (254 nm and 365 nm).

Fluorescence spectra was measured using a fluorescence spectrophotometer (RF-6000, SHIMADZU, Japan). UV-Vis absorbance spectra was measured on a UV-Vis spectrophotometer (V-5800(PC), METASH, China). Fourier transform infrared spectroscopy (FTIR, Thermo, USA) spectra were obtained using potassium bromide pellets after drying. Transmission electron microscopy (TEM, JEM-2100, JEOL, Japan) images were obtained on air-dried ultrathin carbon films. Atomic force microscopy (AFM, Bruker Dimension Icon, Germany) images were captured on drop-casting an aqueous solution on mica plates, completely dried at room temperature. Fluorescence lifetimes and quantum yields were obtained with a fluorescence spectrometer (Spectrofluorometer FS5, UK). DLS measurements were conducted using a Nano Brook 90 Plus PALS (Brookhaven, USA) instrument. Mass spectrometry (MS) spectra were recorded on a Bruker time-of-flight mass spectrometer (Bruker ultra extreme, Germany) with a matrix-assisted laser desorption/ionization source (MALDI-TOF) (matrix: TCNQ). The electron spin resonance (ESR, Bruker EMX plus, Germany) technique was employed to detect ROS generated under irradiation.

RPMI 1640 cell medium, fetal bovine serum (FBS), penicillin-streptomycin, phosphate buffered saline (PBS) at pH 7.4 and 3-(4,5-dimethylthiazol-2-yl)-2,5-diphenyl tetrazolium bromide (MTT), 2',7'-Dichlorodihydrofluorescein diacetate (DCFH-DA) were purchased from Dalian Meilun Biotechnology Co., Ltd (China). The Hoechst 33342 and Lyso-Tracker Green were bought from Beyotime Biotechnology Co., Ltd. The optical density (OD) values were obtained by Enzyme Calibrator (Labserv K3 enzyme standard instrument, Thermo Fisher Technology, Co., Ltd., China). All the other reagents and solvents were provided by Sinopharm Chemical Reagent Co., Ltd.

Methods

Synthesis of HPGQD.

To precisely control the structural configuration of GQD, we designed a synthetic pathway originating from a simple benzene ring. Initially, compound 2 was synthesized using 3-bromoacetophenone (Figure S1, S4-7), and compound 5 was synthesized using 4-bromo-phenylacetic acid (Figure S2, S8-13). As shown in Figure S3, compounds 2 and 5 underwent a Diels-Alder reaction, resulting in the formation of polycyclic aromatic hydrocarbons (PAH) (compound 6) (Figure S3, S14-15). Following this reaction, PGQD was synthesized by dehydrogenating the PAH via a Scholl reaction, with ferric chloride serving as the catalyst. Ultimately, HPGQD, containing functional methoxycarbonyl groups at the edges, was obtained through a hydrolysis reaction.

FL of ROS evaluation.

DCFH-DA (10×10^{-6} mol L^{-1}) was dissolved in DMSO (100 mL) and followed by the addition of NaOH (1 mol L^{-1}) 10 mL solution, and the solution was stirred for 2 h under dark conditions. Subsequently, the pH of the solution was adjusted to 7.4 by the addition of HCl solution (1 mol L^{-1}) to obtain DCFH (10×10^{-6} mol L^{-1}). This solution was stored in the dark and frozen until further use. Following this, an equal volume of DCFH (250 μL) was added to to HPGQD aqueous solution (2.75 mL). Subsequently, the samples were subjected to irradiation with various wavelengths of laser light (1.5 W cm^{-2}). The generated ROS oxidized DCFH to yield 2',7'-Dichlorofluorescein (DCF), resulting in fluorescence emission. The fluorescence spectrum was promptly measured at excitation wavelength (λ_{ex}) of 488 nm and emission wavelength (λ_{em}) of 525 nm.

$^1O_2$ quantum yield measurements.

RB served as the standard photosensitizer, while Na_2-ADPA functioned as a $^1O_2$ capture agent. To initiate the experiment, an aqueous solution of Na_2-ADPA (1 mg mL^{-1}, 60 μL) was introduced into HPGQD aqueous solution (7.5 μmol L^{-1}, 1.5 mL). White light (20 mW cm^{-2}) was employed as the irradiation source. The absorption of Na_2-ADPA at 378 nm was monitored at various irradiation durations to determine the attenuation rate of the photosensitization process. Subsequently, the $^1O_2$ quantum yields of HPGQD in water were computed utilizing the following equation (1):

$$\Phi_{HPGQD}=\frac{\Phi_{RB}\times K_{HPGQD}\times A_{RB}}{K_{RB}\times A_{HPGQD}} \quad (1)$$

ESR of ROS evaluation.

The sample was dispersed in deionized water as a solvent with a concentration of 7.5 μmol L^{-1}, followed by ultrasonic dispersion for 1 min. Subsequently, 30 μL of the sample was withdrawn, to which 50 μL of TEMP (100 mmol L^{-1}) or DMPO (100 mmol L^{-1}) was added and thoroughly mixed. A certain volume of the mixed solution was drawn into a capillary tube, onto which a quartz tube was placed. This assembly was then inserted into the ESR sample chamber and positioned within the ESR resonance cavity. The sample was irradiated with a xenon lamp (300 W) for 30 s to initiate the $^1O_2$

radical test. The ESR signal of the radical TEMPO (2,2,6,6-tetramethyl-1-piperidinyl oxirane) was generated through the reaction of $^1O_2$ with TEMP.

Cellular characterization.

Cell culture. Mouse breast cancer (4T1) cells were cultured in RPMI 1640 cell medium containing 10 % fetal bovine serum and 1 % antibiotic (penicillin, 10,000 U mL^{-1}) at 37 °C in a humidified atmosphere with 5 % CO_2.

MTT assay. Initially, the viability of 4T1 cells was assessed via the MTT assay after a 24 h incubation with varying concentrations of HPGQD. 4T1 cells were cultured in 96-well plates (1×10^4 cells/well) and allowed to culture for 12 h. Following this, the cell culture medium was replaced with HPGQD (0, 0.06, 0.12, 0.23, 0.47, 0.94, 1.88, 3.75, 7.5, 15 μmol L^{-1}) for 6 h. After that, the cells were treated with light (460 nm, 20 mW cm^{-2}) and for an additional 18 h. Upon completion of the incubation period, 20 μL MTT (5 mg mL^{-1}) was added to each well and incubated for 4 h. The medium was then aspirated, and 150 μL DMSO was added to dissolve the crystalline methanogen with shaking for 10 min. The OD of each well was measured at 492 nm using an enzyme marker. The obtained results were expressed as the mean ±SD (n = 3). Cell viability was calculated using the following equation (2):

$$\text{Cell Viability (\%)} = \frac{OD_{sample} - OD_{blank}}{OD_{control} - OD_{blank}} \times 100\% \quad (2)$$

Cellular uptake. The 4T1 cells were seeded at a density of 1.0×10^5 cells per well and cultured in confocal dishes for 12 h. Initially, the culture medium containing HPGQD (3 μmol L^{-1}, 1 mL) was added to the cells and allowed to incubate for 2, 4, and 6 h, followed by washing with PBS. Subsequently, 1 mL of Lyso-Tracker Green (10×10^{-6} mol L^{-1}) was added to the cells and incubated for 15 min, after which they were washed again with PBS. Next, the cells were fixed with 4 % paraformaldehyde and stained with Hoechst 33342. Finally, the cells were washed and observed using a confocal laser scanning microscope (CLSM, Carl Zeiss, LSM 710, Germany) to ascertain the cellular uptake of HPGQD.

Detection of ROS. 4T1 cells were seeded at a density of 1.0×10^5 cells per well and cultured in confocal dishes for 12 h. Initially, the cells were exposed to medium containing HPGQD (3 μmol L^{-1}, 1 mL) for 2, 4 and 6 h following a wash with PBS. Subsequently, 1 mL of DCFH-DA (10×10^{-6} mol L^{-1}) and incubated for 15 min, after which the cells were washed again with PBS. For the control group, no irradiation was applied. Following this, the cells were irradiated with 460 nm (20 mW cm^{-2}) for 30 s and washed with PBS. The cells were then fixed with 4 % paraformaldehyde and stained with Hoechst 33342. Finally, the cells were washed and observed using CLSM.

For the quantitative analysis of intracellular ROS, 4T1 cells were treated identically to the CLSM procedure to observe intracellular ROS. After the light illumination, the cells were digested and collected, then dispersed in 0.2 mL of PBS. Subsequently, the ROS levels of HPGQD were quantified

using flow cytometry (FCM, BD C6 PLUS, USA), with an excitation wavelength of 488 nm and an emission filter of 525 nm.

In vivo PDT efficacy.

Animal model. The female nude mice (5-6 weeks old) were procured from Liaoning Changsheng Biotechnology Co., Ltd (Changchun, China). Subcutaneous tumor models were established by injecting 4T1 cells (1×10^7 cells) into the right thigh of the mice. Following one week of acclimatization, the nude mice were randomly allocated into 4 groups (n=5) for subsequent experiments. All animal-related procedures were conducted in compliance with the guidelines approved by the Experimental Animal Center of Wuhan University of Science and Technology (Animal Use Certificate No. 2024058). Additionally, all animal experiments adhered to the Regulations on the Administration of the Trade Fair for Laboratory Animals sanctioned by the State Council of the People's Republic of China.

***In vivo* fluorescence imaging.** To assess the *in vivo* fluorescence imaging capability and retention duration of HPGQD in nude mice, HPGQD (100 μL, 150 μmol L^{-1}) was injected around the subcutaneous tumors of the nude mice following one week of feeding. Subsequently, fluorescence signal variations within the tumors of the nude mice were monitored at specific time intervals (0, 12, 24, 48, and 72 h) using a small animal *in vivo* 3D optical imaging system (PerkinElmer, IVIS Spectrum, China) positioned at the tumor site.

***In vivo* PDT effect.** The nude mice were injected peritumorally with HPGQD (100 μL, 150 μmol L^{-1}). The tumors were injected subcutaneously every 3 days and irradiated every 2 days using a laser (460 nm, 1.5 W cm^{-2}, 30 s). Body weight and tumor volume of nude mice were monitored daily for up to 14 days. Two-dimensional tumor volumes were measured with vernier calipers and calculated by the following Equation (3):

$$V=\frac{L\times W^2}{2} \tag{3}$$

where L represents the longest diameter of the tumor and W represents the shortest diameter of the tumor. At the 14th day post-treatment, the mice were euthanized. Whole blood cell analysis was conducted using periocular blood sampling. Tumors were excised and weighed, and tumor tissues from each group of mice were subjected to HE staining and TUNEL staining analysis. Additionally, major organ tissues (heart, liver, spleen, lung, and kidney) were dissected for HE staining analysis.

HE Staining for Paraffin Sections. The HE staining process for paraffin sections begins with dewaxing and hydration. The sections are immersed sequentially in xylene for two 15-min intervals, followed by absolute ethanol for two 5-min intervals, then 90% alcohol and 75% alcohol for 5 min, respectively, with final rinsing in tap water. Next, the nuclei are stained with hematoxylin for 10 min, followed by rinsing in tap water, differentiation with 1% hydrochloric acid, rinsing again, bluing with 1% ammonia water, and final rinsing in tap water. The cytoplasm is then stained with eosin for 3 min. Dehydration and mounting are achieved by immersing the sections in absolute ethanol for two 5-min

intervals, followed by xylene for two 5-min intervals, and finally mounting with neutral balsam. Under the microscope, carefully observe and record the staining results to assess the characteristics of tissue structure and changes in cell morphology.

TUNEL (Green Fluorescence) Staining. The TUNEL staining procedure for paraffin sections involves several steps. First, dewax the sections and hydrate them by immersing them in xylene for two 15-min intervals, followed by absolute ethanol for two 5-min intervals, then 90% alcohol for a brief period, and finally 75% alcohol for 5 min, with rinsing in tap water. After rinsing with pure water, a histochemical pen is used to draw a circle around the tissue to prevent the incubation solution from flowing away during subsequent steps, followed by washing with PBS. Next, prepare a working solution by diluting protease K from the kit with PBS at a ratio of 1:9 and incubate at 37°C for 20 min, followed by three PBS washes, each lasting 5 min. Prepare a permeabilization solution and incubate at room temperature for 10 min, with three subsequent PBS washes. Then, mix TdT enzyme, CF488-dUTP green fluorescent reaction mixture, and EB equilibration buffer from the kit in the ratio of 1:5:50 to prepare an appropriate amount of incubation solution, and incubate in the dark at 37°C for 1 to 1.5 h or at 4°C overnight. Following three PBS washes, stain the nuclei with DAPI by incubating in the dark at room temperature for 20 to 30 min, with a final PBS wash. Finally, mount the sections using an anti-fade mounting medium and observe and photograph them under a microscope.

Synthetic steps of compound 2.

The synthesis of compound 2. A synthetic method used to prepare compound 2 is schematically summarized in Figure S1.

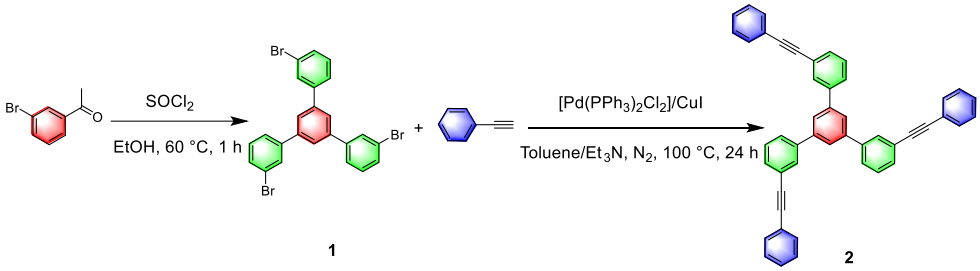

Figure S1. Synthesis route to compound 2.

Synthesis steps of compound 1.

Using a syringe, sulfoxide chloride (8.92 g, 75 mmol) was slowly added to a stirred solution of 3-bromoacetophenone (8.96 g, 45 mmol) in anhydrous ethanol (13 mL, 225 mmol). The mixture was stirred at reflux temperature for 1 h. Samples were taken for TLC and the reaction was completed when the raw material point disappeared. The reaction temperature was lowered to room temperature and neutralized with a saturated sodium bicarbonate solution. The cooled solid was washed with water, ether, and ethanol in turn, and dried by rotary evaporation to give compound 1 (6.90 g, 85 %) as a light yellow solid. ^{1}H NMR (600 MHz, $CDCl_3$): δ 7.82 (s, 3H), 7.71 (s, 3H), 7.60 (d, *J* = 7.8 Hz, 3H), 7.54 (d, *J* = 7.9 Hz, 3H), 7.36 (t, *J* = 7.8 Hz, 3H). ^{13}C NMR (150 MHz, $CDCl_3$): δ 143.53, 141.21, 130.75, 130.43, 130.33, 125.96, 125.51, 123.05. APCI-FTMS (m/z): $[M-H]^-$ calcd. for **$C_{24}H_{15}Br_3$**: 542.8808, found: 542.8804.

Synthesis steps of compound 2.

Compound 1 (1.08 g, 2 mmol), Phenylacetylene (1.02 g, 10 mmol), Bis(triphenylphosphine) palladium (II) dichloride (0.12 g, 0.172 mmol) and cuprous iodide (0.014 g, 0.072 mmol) were added together. This system was reacted at 100 °C for 24 h under N_2 atmosphere. After the reaction was detected by TLC, the solid was obtained by filtration and washed three times with methanol, the solvent was removed by rotary evaporation and the residue was purified on a silica gel column with a mixture of petroleum ether and ethyl acetate (50/1, v/v) to give compound 2 (1.04 g, 86 %) as a pale yellow solid. ^{1}H NMR (600 MHz, $CDCl_3$): δ 7.91 (s, 3H), 7.84 (s, 3H), 7.70 (d, J = 7.7 Hz, 3H), 7.60 – 7.56 (m, 9H), 7.49 (t, J = 7.7 Hz, 3H), 7.38 – 7.34 (m, 9H). ^{13}C NMR (150 MHz, $CDCl_3$): δ 141.68, 141.06, 131.67, 130.76, 130.46, 129.13, 128.94, 128.35, 127.28, 125.32, 123.91, 123.13, 89.76, 89.25. APCI-FTMS (m/z): $[M+H]^+$ calcd. for **$C_{48}H_{30}$**: 607.2415, found: 607.2420.

Synthetic steps of compound 5.

The synthesis of compound 5. A synthetic method used to prepare compound 5 is schematically summarized in Figure S2.

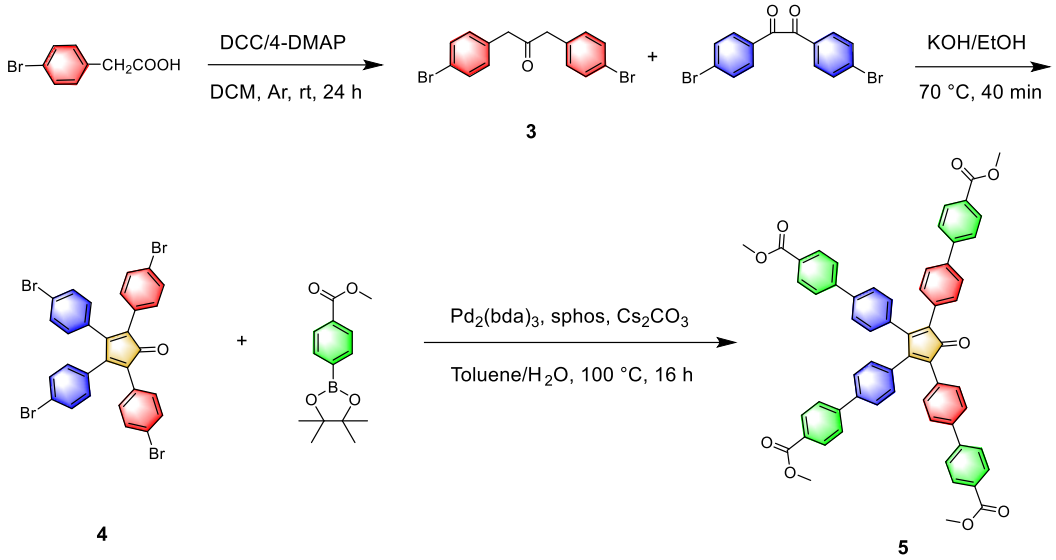

Figure S2. Synthesis route to compound 5.

Synthesis steps of compound 3.

A solution of 4-bromophenylacetic acid (6.45 g, 30 mmol) in CH_2Cl_2 (75 mL) was added dropwise to a mechanically stirred solution of dicyclohexylcarbodiimide (6.19 g, 30 mmol) and 4-(dimethylamino) pyridine (0.92 g, 7.5 mmol) in the CH_2Cl_2 (70 mL). The reaction was allowed to proceed for 24 h at room temperature under N_2 atmosphere. After the reaction was detected by TLC, the dicyclohexylurea was removed by filtration and the filtrate was processed by rotary evaporation. The residue was purified through a silica gel column using a mixture of petroleum ether and dichloromethane solvents (v/v, 1:3) to give compound 3 (7.73 g, 70 %) as a yellow solid. ^{1}H NMR (600 MHz, $CDCl_3$): δ 7.45 (d, J = 8.1 Hz, 4H), 7.01 (d, J = 8.1 Hz, 4H), 3.68 (s, 4H). ^{13}C NMR (150 MHz, $CDCl_3$): δ 204.22, 132.57, 131.83, 131.14, 121.24, 47.93. APCI-FTMS (m/z): $[M-H]^-$ calcd. for **$C_{15}H_{12}Br_2O$**: 366.9182, found: 366.9168.

Synthesis steps of compound 4.

Compound 3 (1.84 g, 5 mmol),1,2-Bis(4-bromophenyl) ethane-1,2-dione (1.84 g, 5 mmol) dissolved in EtOH (7 mL) was added to a stirred solution of potassium hydroxide (0.28 g, 5 mmol) dissolved in EtOH (3 mL). The reaction was refluxed at 70 °C for 40 min. Cool to room temperature, the reaction was filtered, washed with EtOH, and dried under vacuum to give compound 4 (2.91 g, 83 %) as a purple-black solid.^{1}H NMR (600 MHz, $CDCl_3$): δ 7.38 (dd, 8H), 7.06 (d, *J* = 8.5 Hz, 4H), 6.77 (d, *J* = 8.5 Hz, 4H). ^{13}C NMR (150 MHz, $CDCl_3$): δ 198.75, 153.05, 131.75, 131.55, 131.54, 131.13, 130.74, 128.92, 124.94, 123.57, 122.44. APCI-FTMS（m/z): $[M-H]^-$ calcd. for **$C_{29}H_{16}Br_4O$**: 699.7894, found: 699.7910.

Synthesis steps of compound 5.

Compound 4 (420 mg, 0.6 mmol), Methyl 4-(4,4,5,5-tetramethyl-1,3,2-dioxaborolan-2-yl) benzoate (1.89 g, 7.2 mmol), $Pd_2(dba)_3$ (220 mg, 0.24 mmol), Sphos (197 mg, 0.48 mmol) and Cs_2CO_3 (2.346 g, 7.2 mmol) in toluene (20 mL) and H_2O (10 mL) were stirred at 100 °C for 16 h under N_2. Then the mixture was filtered and washed with ethyl acetate. The crude product was evaporated by spin and purified by silica gel column chromatography using petroleum ether/ethyl acetate (v/v, 5:1) as eluent to give compound 5 (265 mg, 48 %) as a purple-black solid.^{1}H NMR (600 MHz, $CDCl_3$): δ 8.09 (d, *J* = 5.3 Hz, 8H), 7.66 (t, 8H), 7.55 (dd, *J* = 17.5, 8.1 Hz, 8H), 7.40 (d, *J* = 8.1 Hz, 4H), 7.13 (d, *J* = 7.9 Hz, 4H), 3.93 (s, 12H). ^{13}C NMR (150 MHz, $CDCl_3$): δ 199.76, 166.91, 166.80, 153.99, 144.88, 144.30, 140.09, 138.99, 132.72, 130.67, 130.49, 130.15, 130.13, 130.09, 130.07, 129.31, 128.98, 126.99, 126.91, 126.82, 125.34, 52.15, 52.10. APCI-FTMS (m/z): $[M+H]^+$ calcd. for **$C_{61}H_{44}O_9$**: 921.3058, found: 921.3082.

Synthetic steps of compound HPGQD.

The synthesis of compound HPGQD. A synthetic method used to prepare HPGQD is schematically summarized in Figure S3.

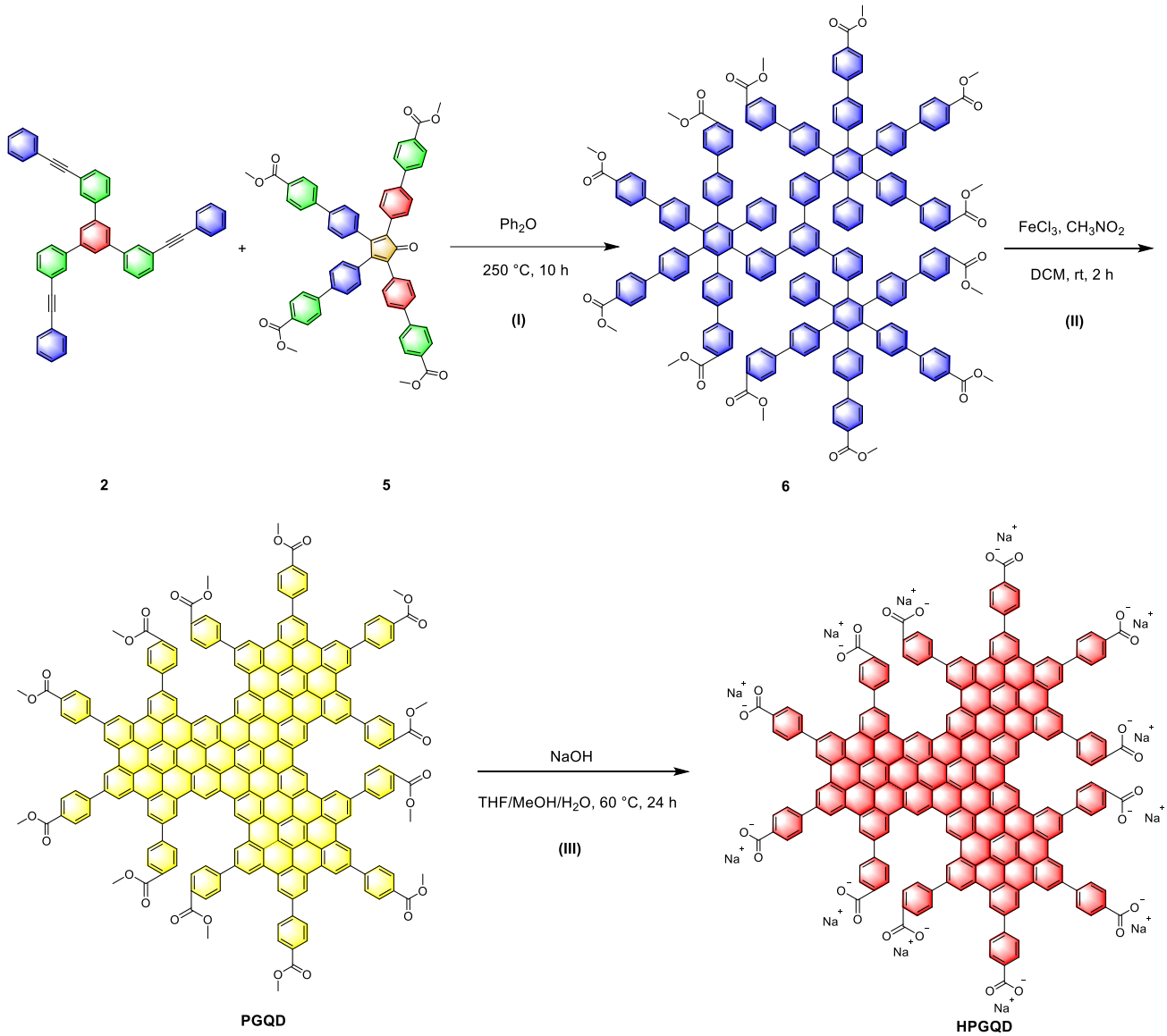

Figure S3. Synthesis route to HPGQD.

Synthesis steps of compound 6.

Compound 2 (60 mg, 0.1 mmol), and **compound 5** (304 mg, 0.33 mmol) were added together to Ph_2O (10 mL) and stirred at 250 °C for 10 h. After cooling to room temperature, the mixture was washed with EtOH and then the mixture was filtered to obtain the crude product, evaporated by spin evaporation, and purified by silica gel column chromatography with petroleum ether/ethyl acetate (v/v, 15:1) as eluent to give compound 6 (112 mg, 34 %) as a dark yellow solid. ^{1}H NMR (600 MHz, $CDCl_3$): δ 8.08 (d, J = 6.1 Hz,12H), 7.96 (t, J = 8.8 Hz, 9H), 7.86 – 7.78 (m, 6H), 7.70 – 7.62 (m, 12H), 7.58 – 7.39 (m, 48H), 7.35 – 7.29 (m, 15H), 7.22 – 7.09 (m, 24H), 3.93 (d, J = 3.6 Hz,36H). ^{13}C NMR (150 MHz, CD_2Cl_2/CS_2): δ 166.63, 166.60, 166.58, 144.81, 144.74, 144.70, 142.70, 142.18, 141.39, 141.24, 140.99,

140.85, 140.64, 140.60, 140.55, 140.42, 140.30, 140.24, 140.17, 139.44, 136.89, 136.87, 136.75, 132.40, 132.30, 132.20, 132.14, 131.70, 131.68, 131.66, 131.63, 131.01, 130.90, 130.76, 130.70, 130.56, 130.17, 129.95, 129.93, 129.89, 129.09, 128.97, 128.91, 128.81, 128.55, 127.46, 127.34, 127.14, 126.64, 126.63, 126.61, 126.54, 126.50, 125.77, 125.71, 125.60, 125.39, 124.80, 124.73, 124.52, 123.99, 123.90, 123.25, 51.92, 51.87. MALDI-TOF-MS (m/z): $[M+H]^+$ calcd. for $\mathbf{C_{228}H_{162}O_{24}}$: 3286.28, found:3286.28. (matrix: TCNQ).

Synthesis steps of compound PGQD.

The anhydrous ferric chloride (487 mg, 3 mmol) dissolved in CH_3NO_2 (75 mL) was slowly added to **compound 6** (100 mg, 0.03 mmol) dissolved in CH_2Cl_2 (50 mL) and stirred with N_2 bubbling for 2 h at room temperature. At the end of the reaction, compound PGQD (112 mg, 34 %) was washed with MeOH and recrystallized to give a brown solid. MALDI-TOF-MS (m/z): $[M+Na]^+$ calcd. for $\mathbf{C_{228}H_{114}O_{24}}$: 3260.40, found:3260.39. (matrix: TCNQ).

Synthesis steps of compound HPGQD.

PGQD (100 mg, 0.03 mmol) was dissolved in 20 mL of THF/MeOH/H_2O (5/5/10 mL), and NaOH (75 mg, 1.85 mmol) was added. The mixture was stirred at 60 °C for 24 h. The crude product was then dialyzed (500 Da) for 12 h with three water changes. It was then spin evaporated and dried under vacuum to give a brown solid (91 mg, 91 %).

NMR of compound 1-6.

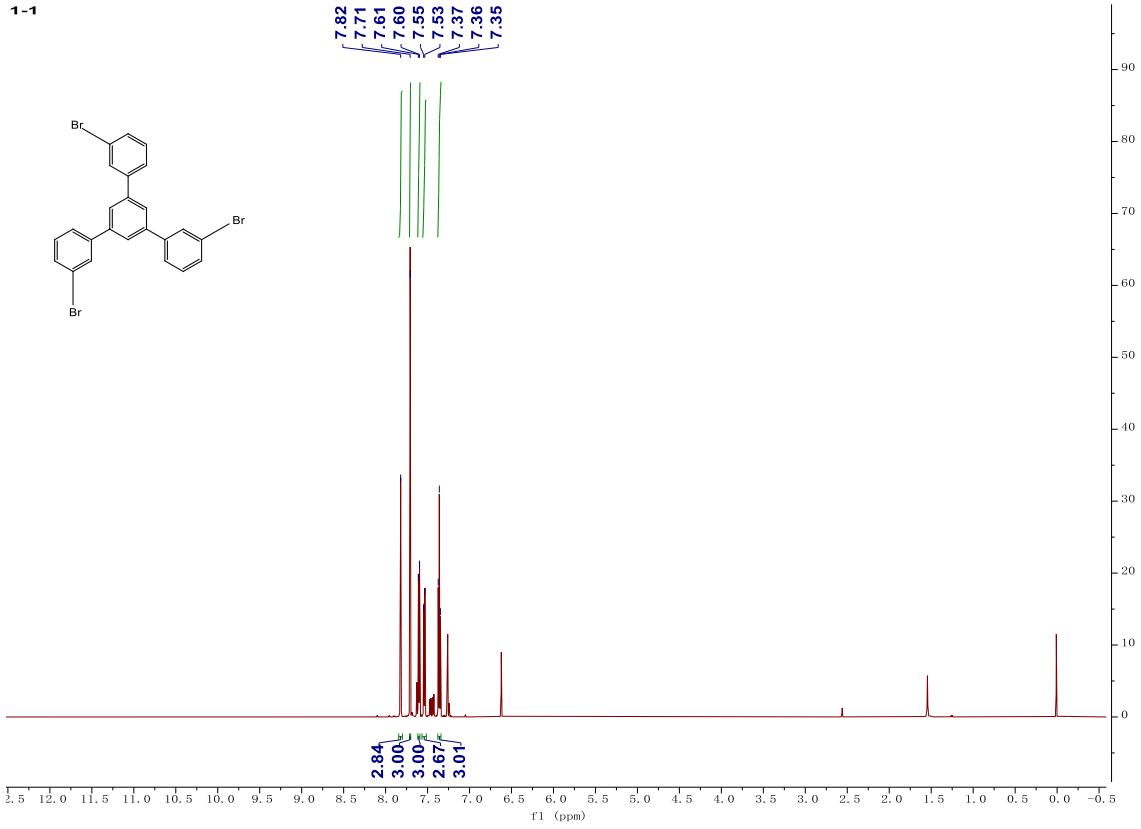

Figure S4. ^{1}H NMR of compound 1.

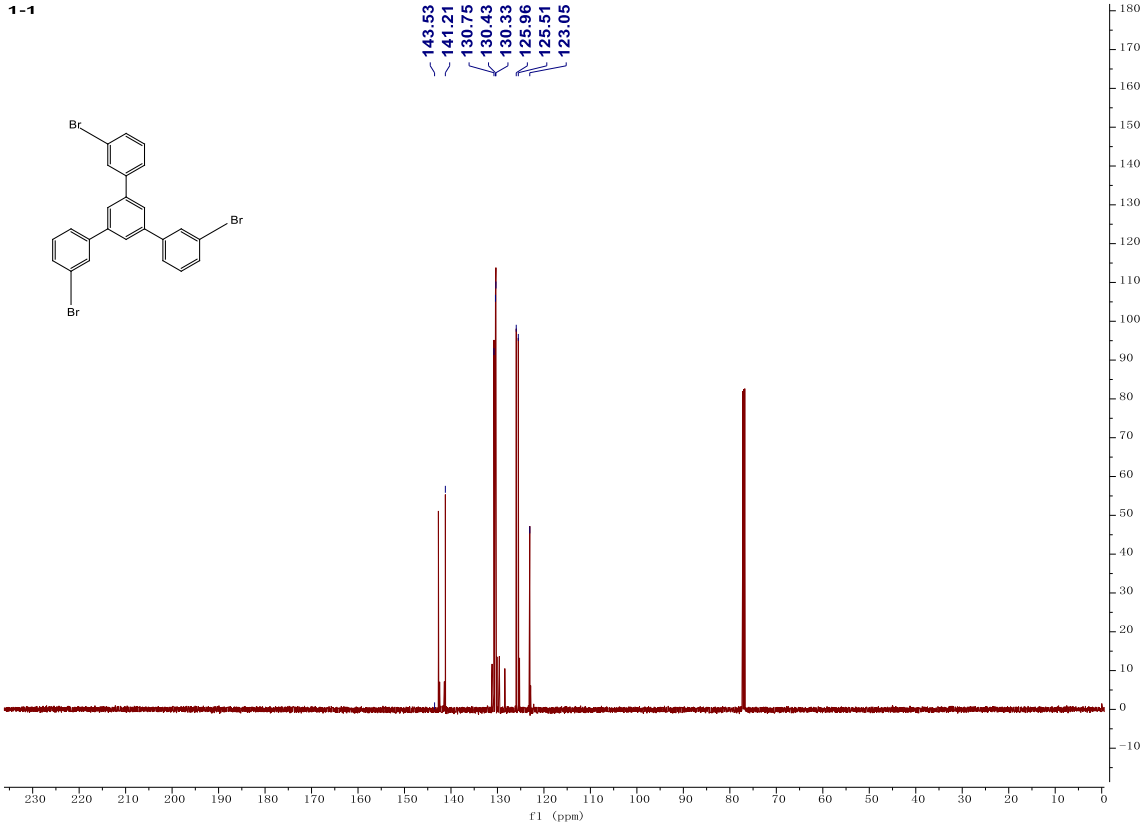

Figure S5. ^{13}C NMR of compound 1.

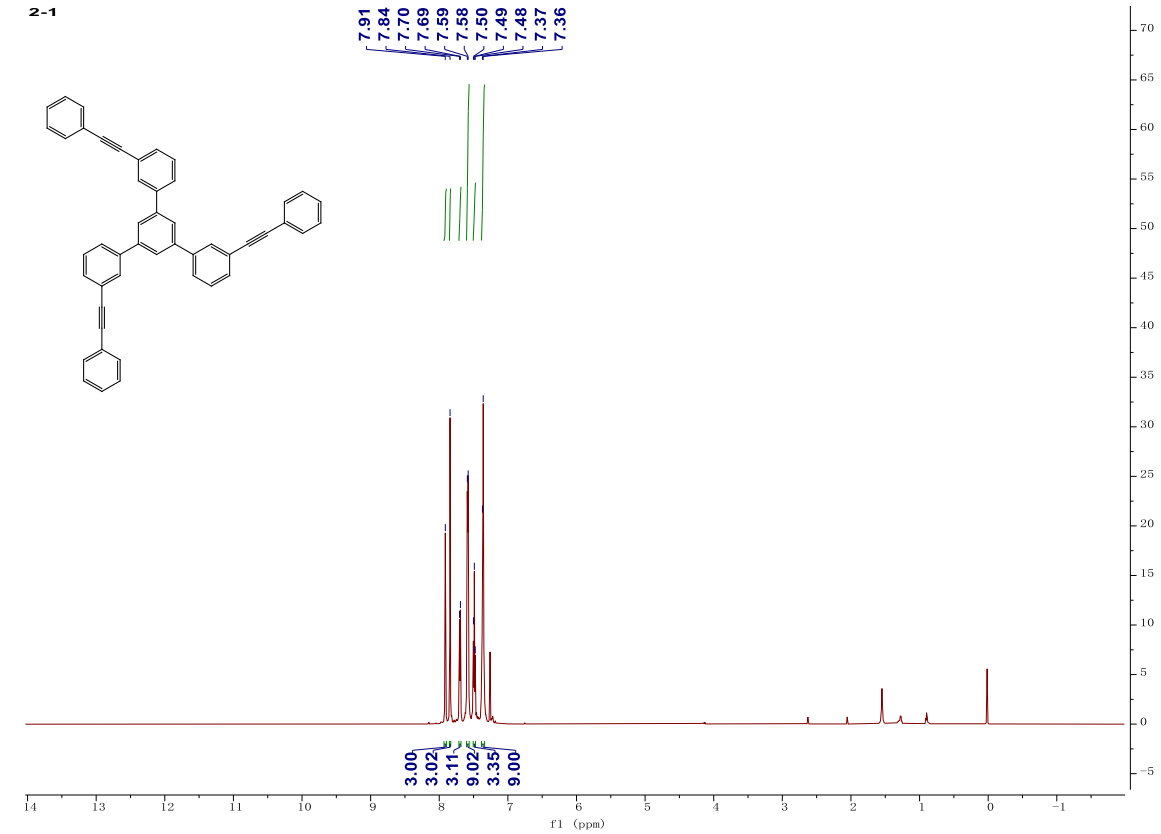

Figure S6. ^{1}H NMR of compound 2.

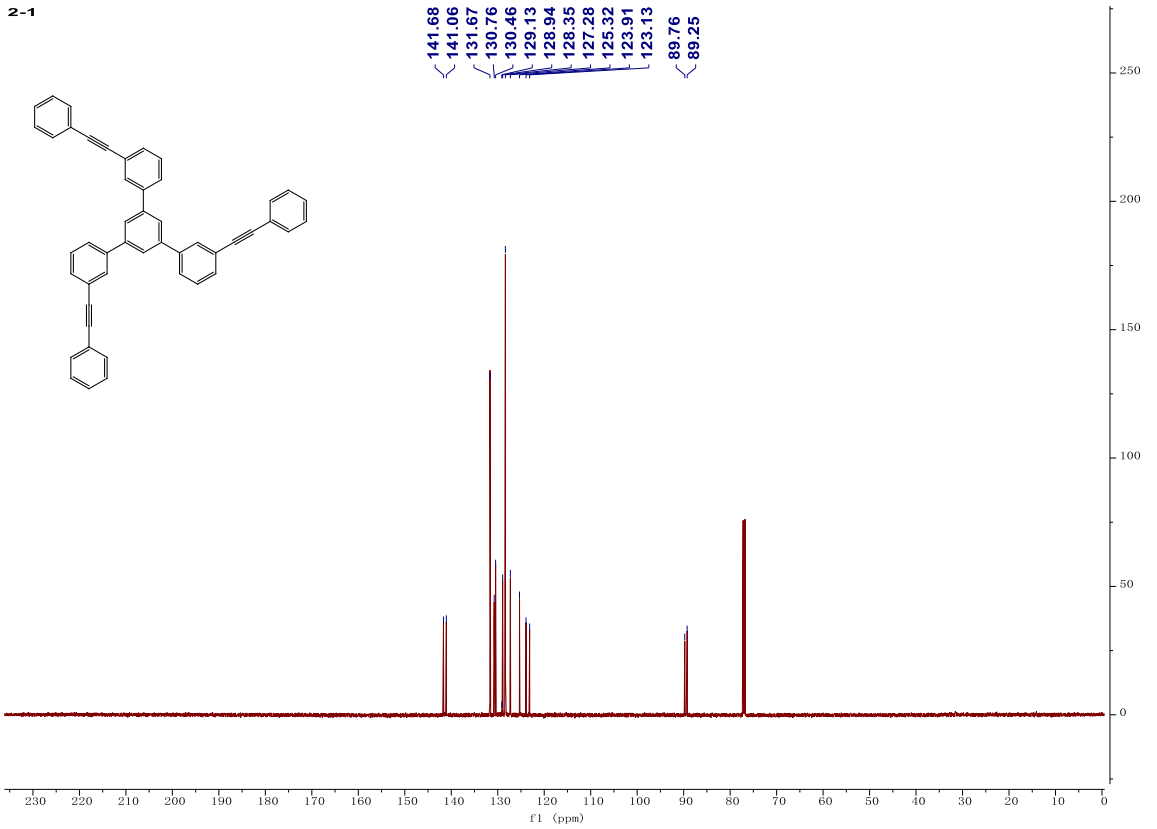

Figure S7. ^{13}C NMR of compound 2.

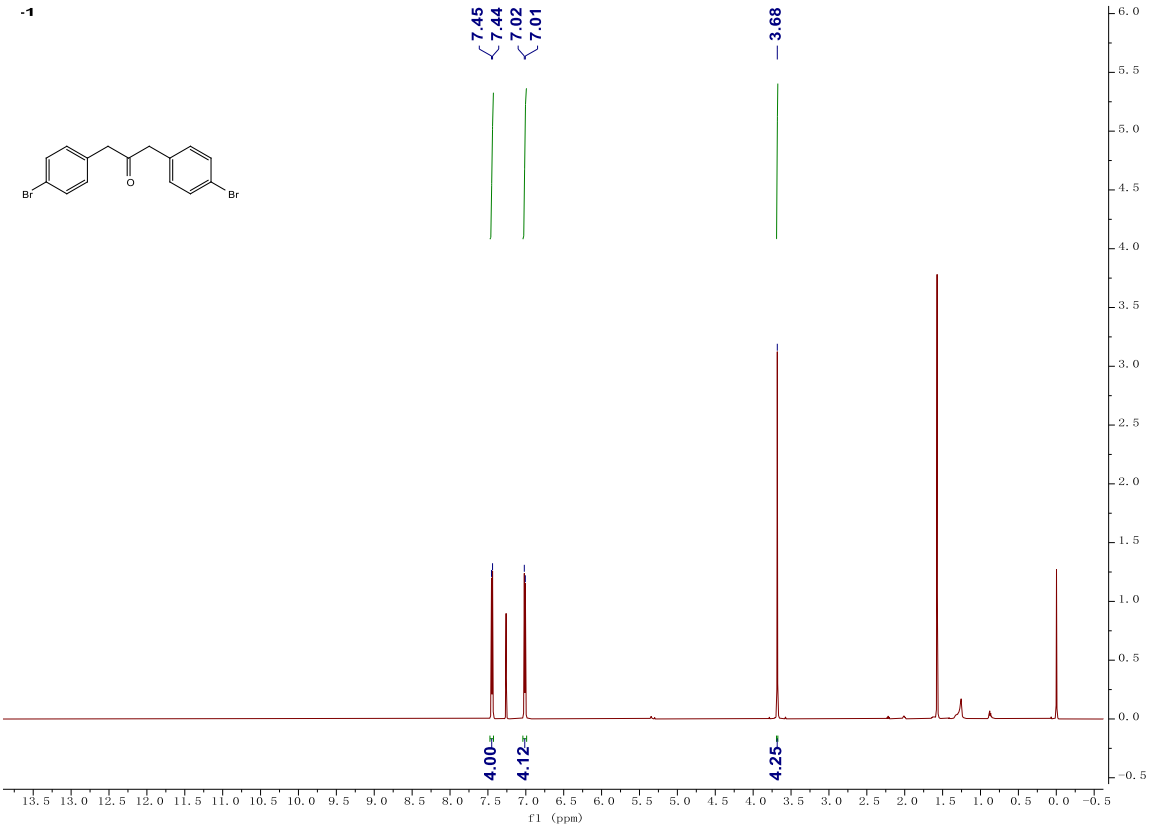

Figure S8. ^{1}H NMR of compound 3.

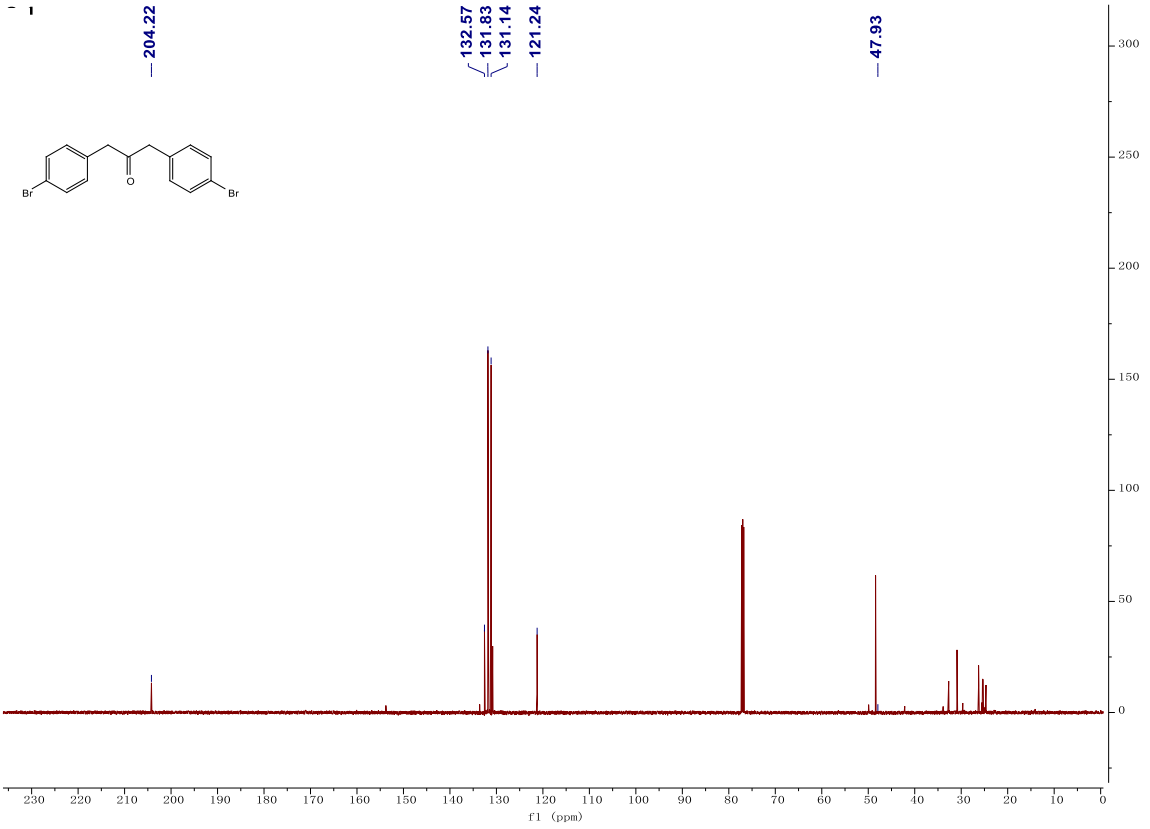

Figure S9. ^{13}C NMR of compound 3.

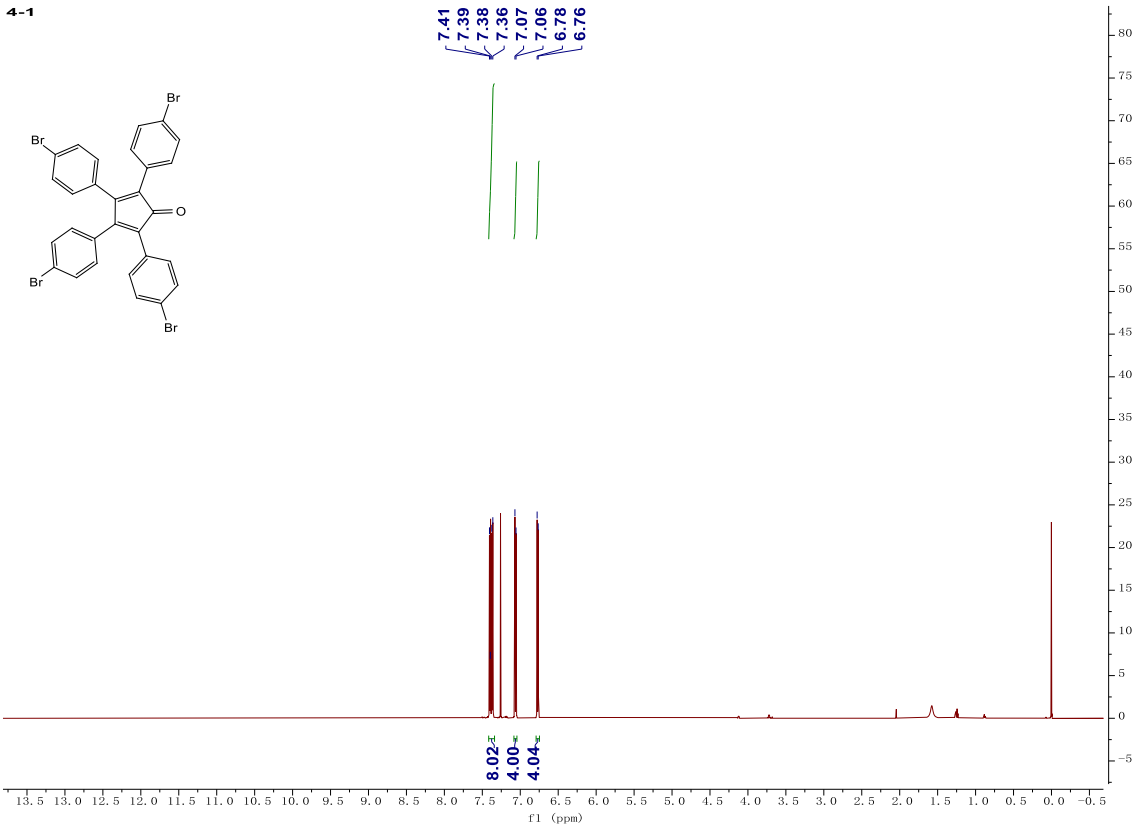

Figure S10. ^{1}H NMR of compound 4.

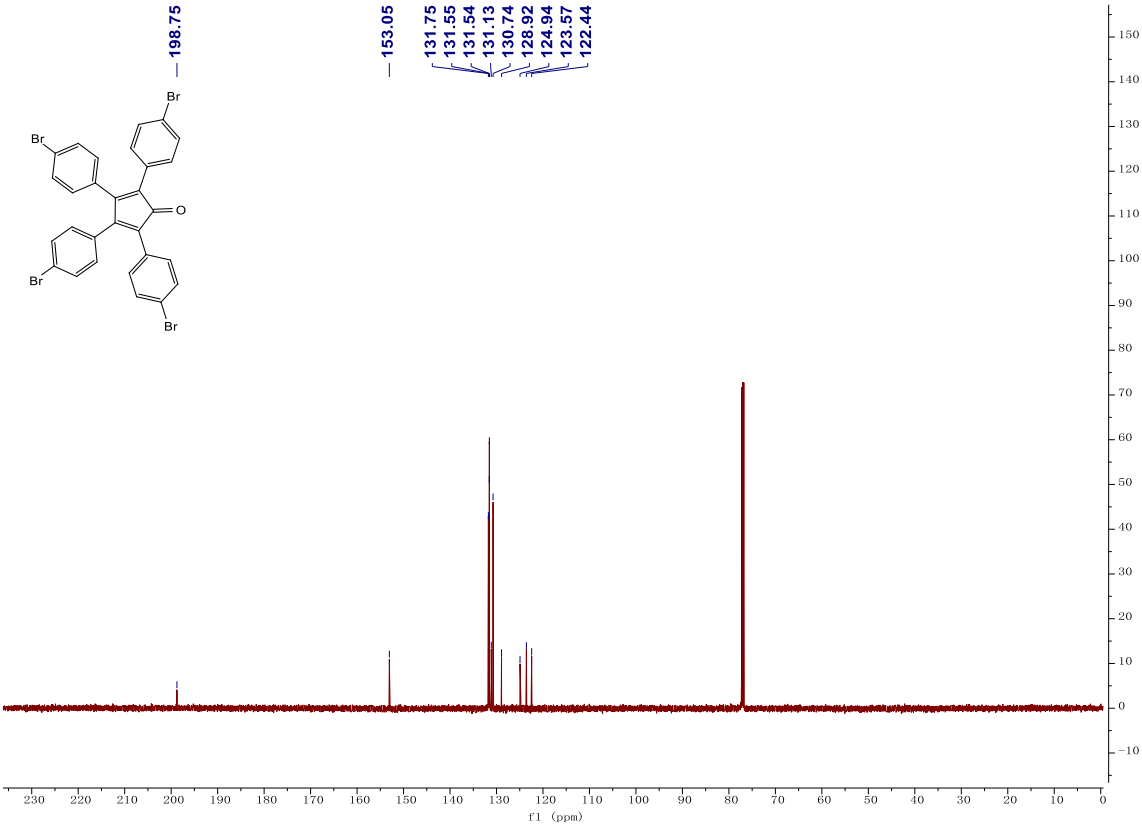

Figure S11. ^{13}C NMR of compound 4.

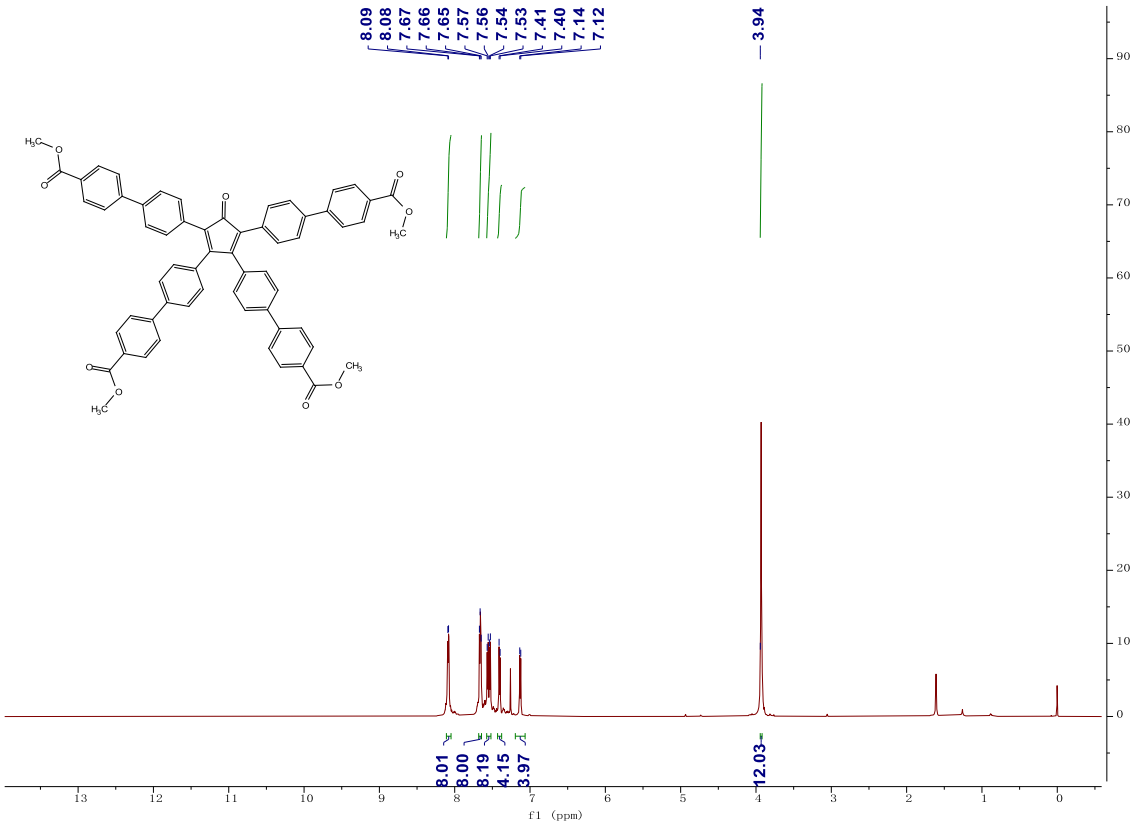

Figure S12. ^{1}H NMR of compound 5.

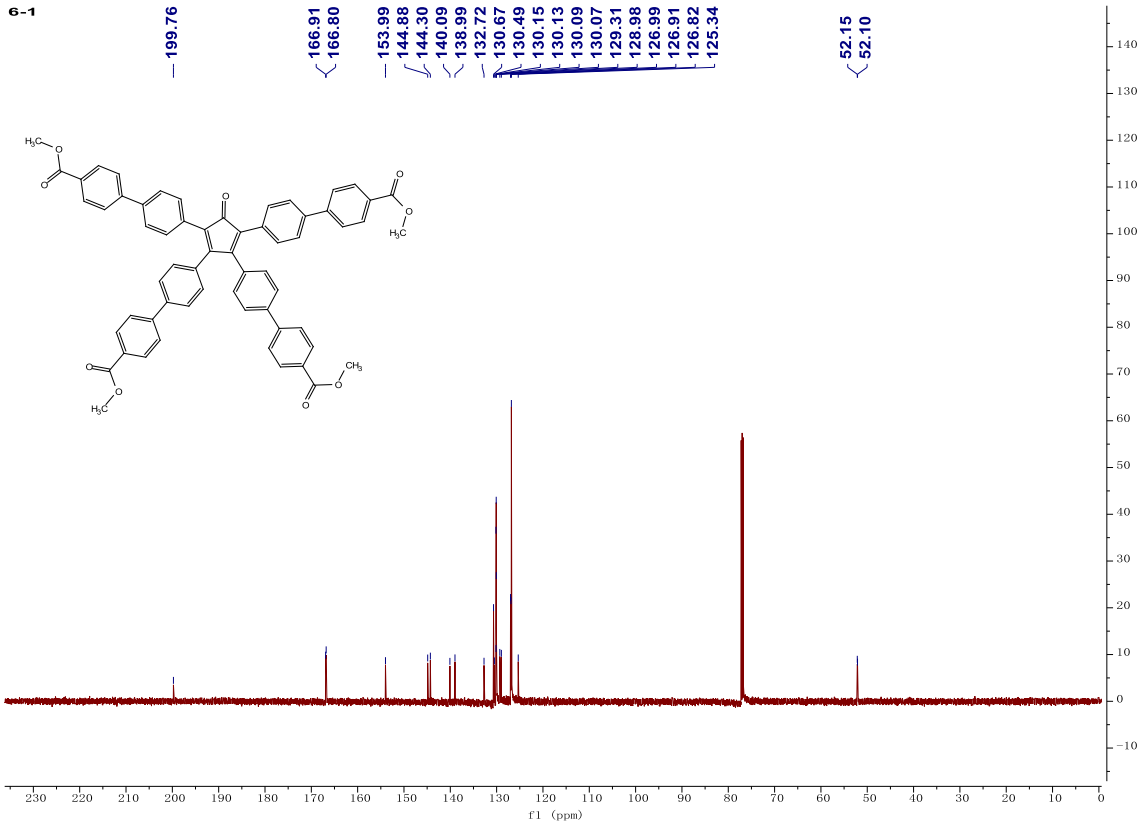

Figure S13. ^{13}C NMR of compound 5.

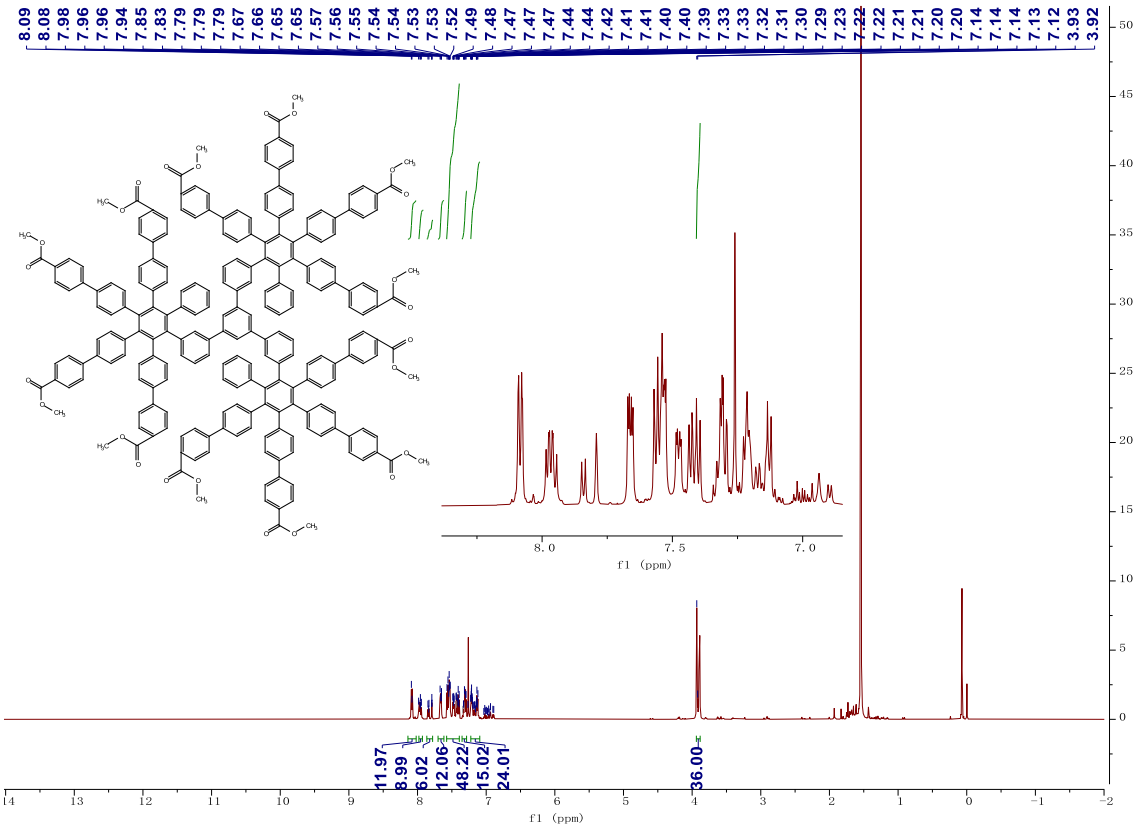

Figure S14. ^{1}H NMR of compound 6.

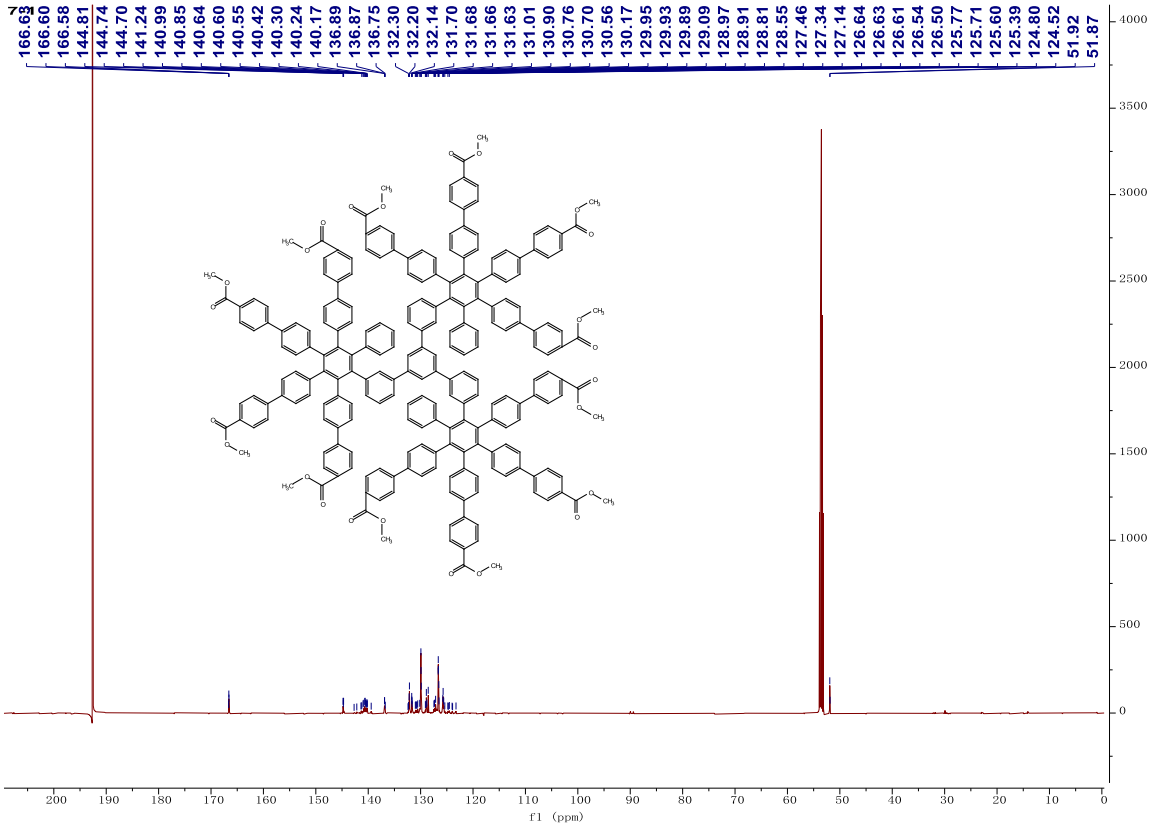

Figure S15. ^{13}C NMR of compound 6.

Mass Spectra of compound 1-6.

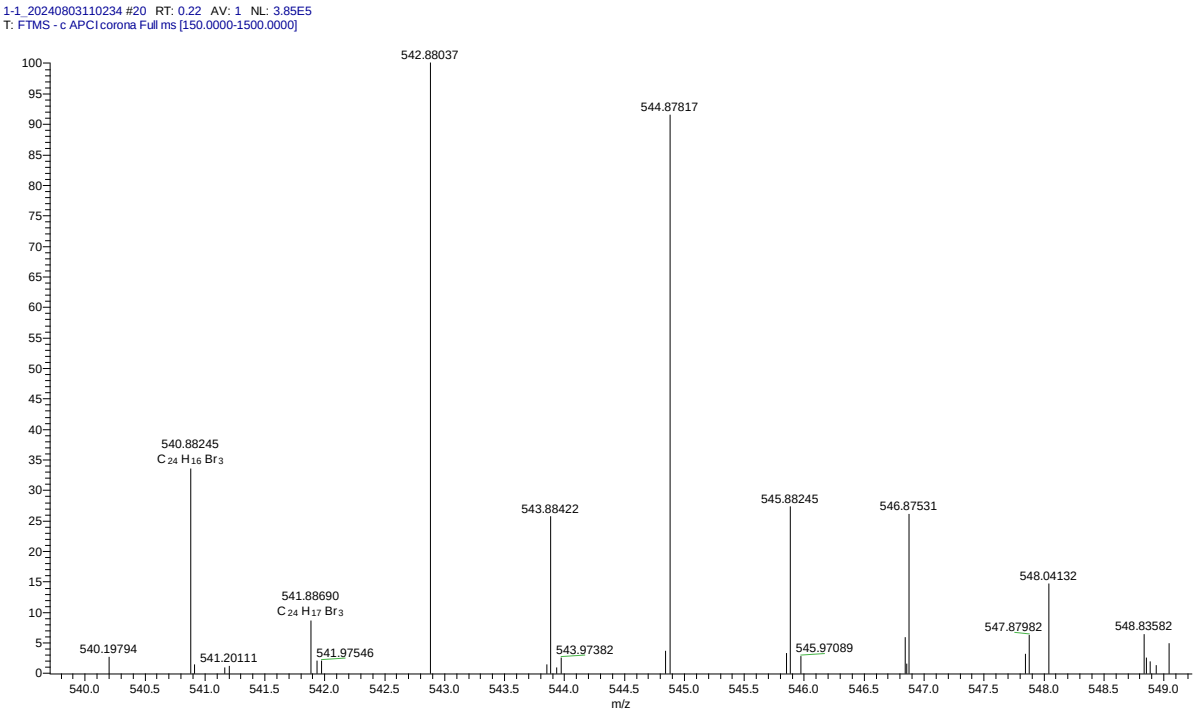

Figure S16. APCI-FTMS spectra of compound 1.

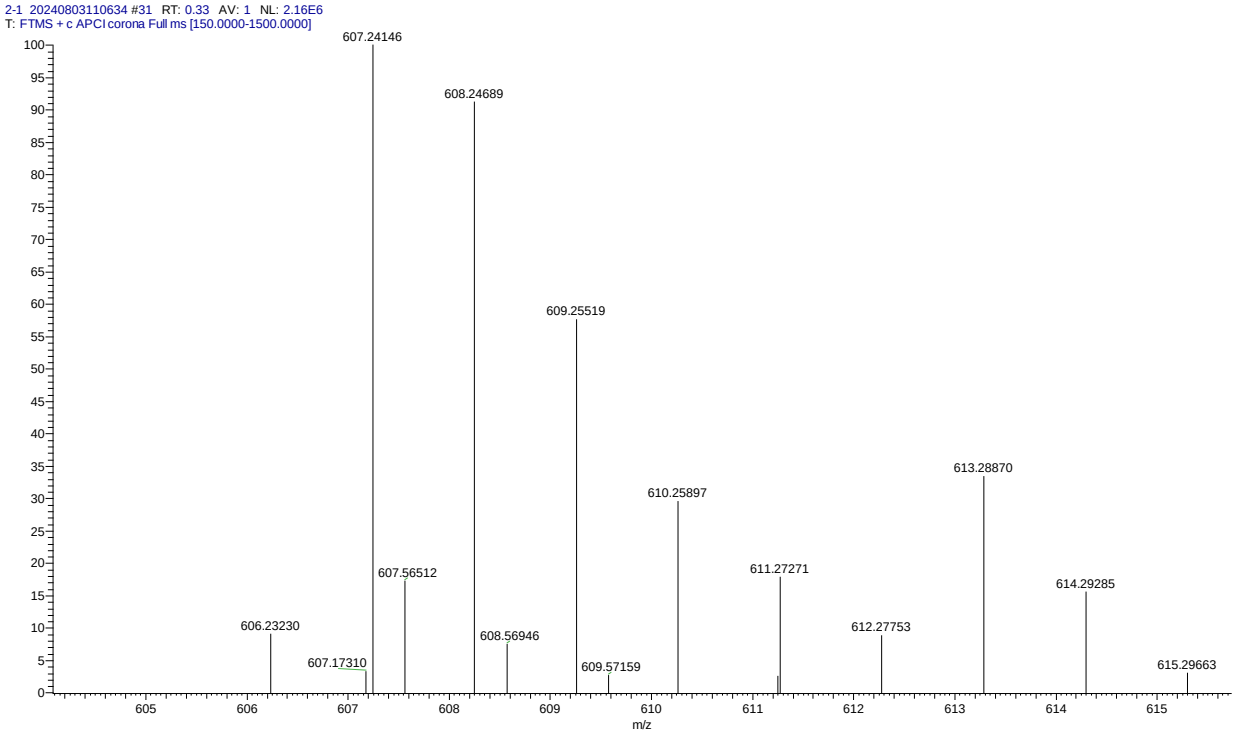

Figure S17. APCI-FTMS spectra of compound 2.

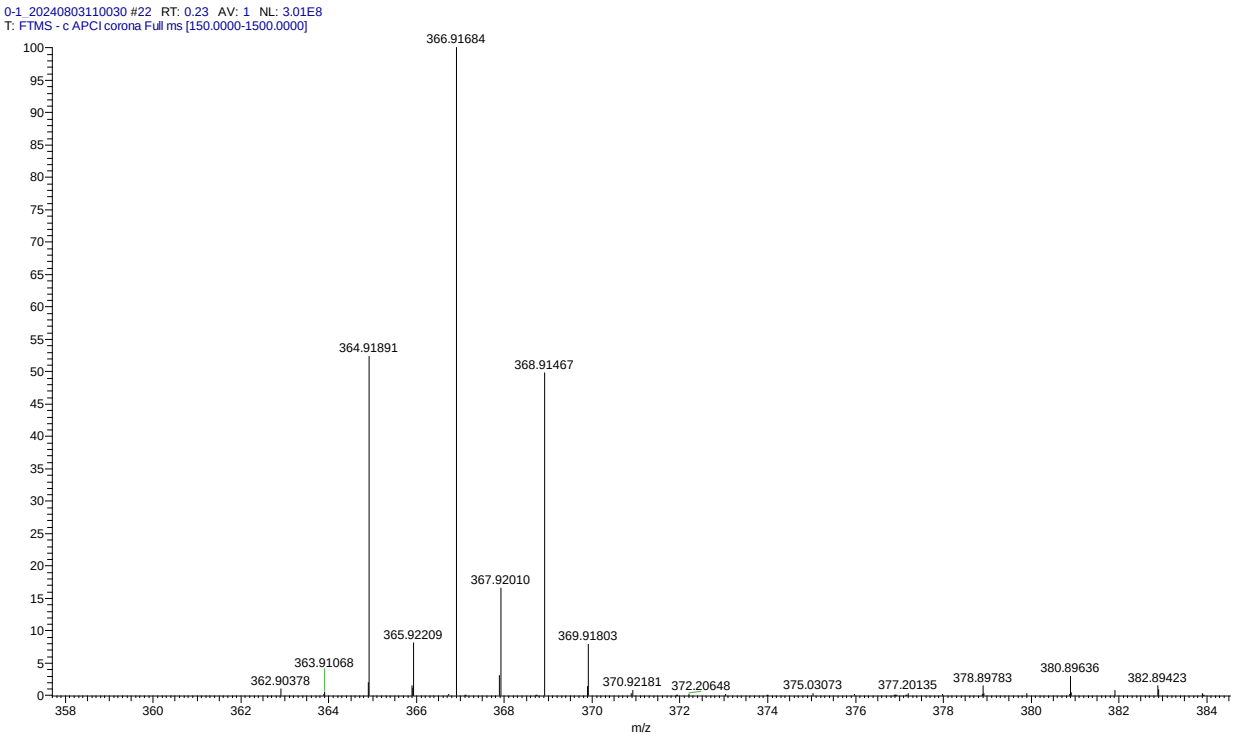

Figure S18. APCI-FTMS spectra of compound 3.

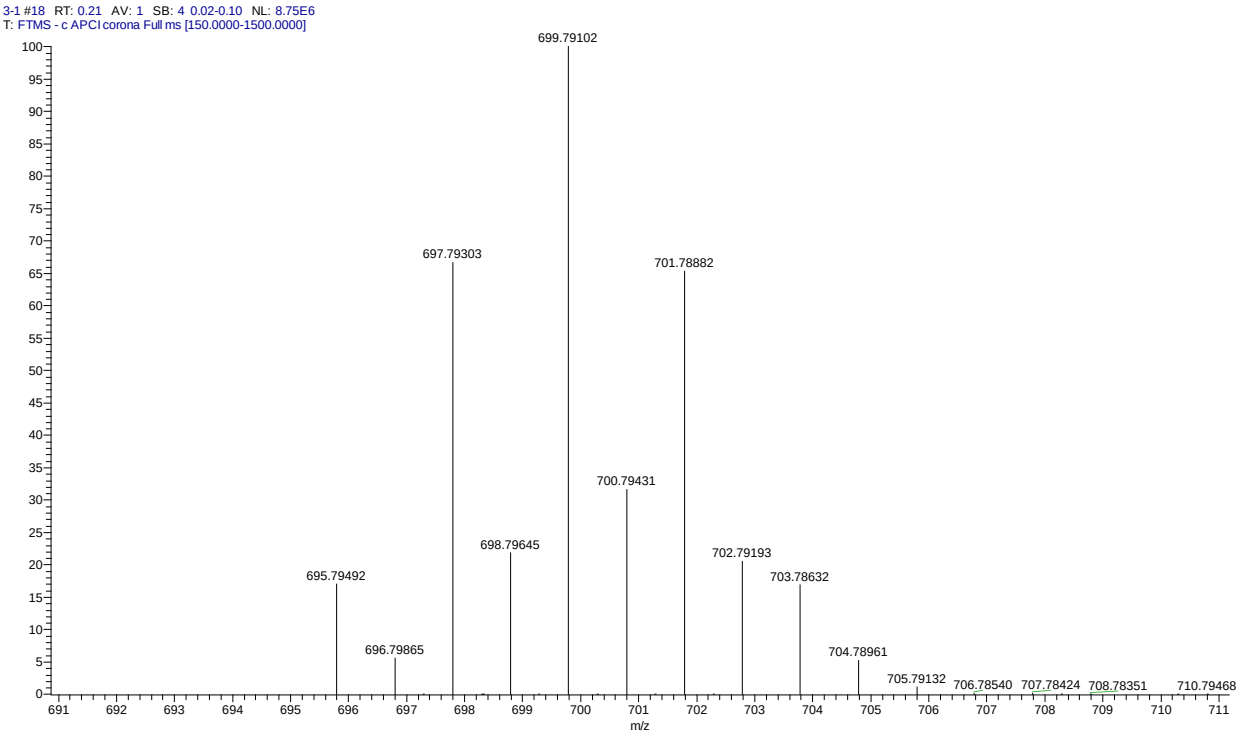

Figure S19. APCI-FTMS spectra of compound 4.

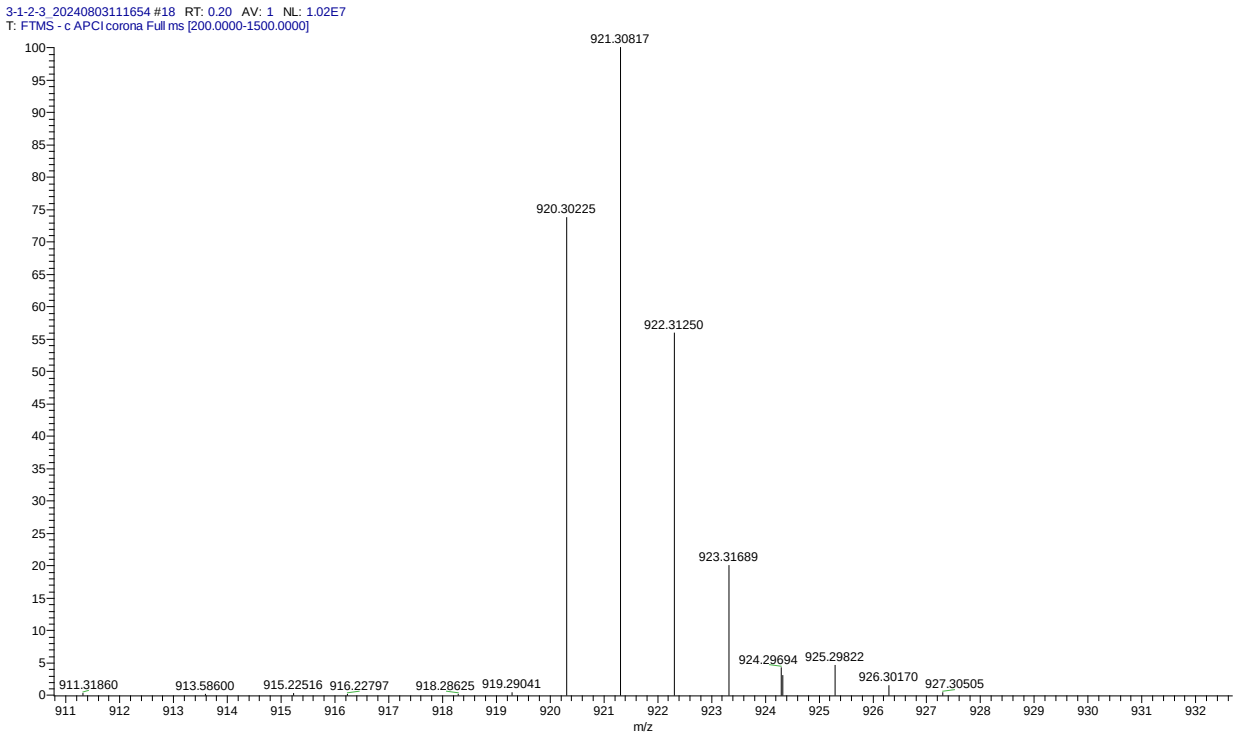

Figure S20. APCI-FTMS spectra of compound 5.

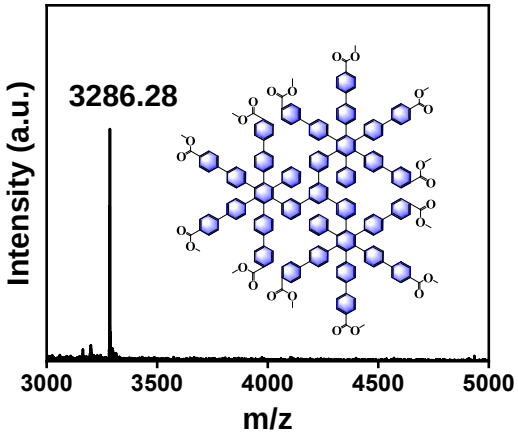

Figure S21. MALDI-TOF-MS spectra of compound 6.

Synthetic details.

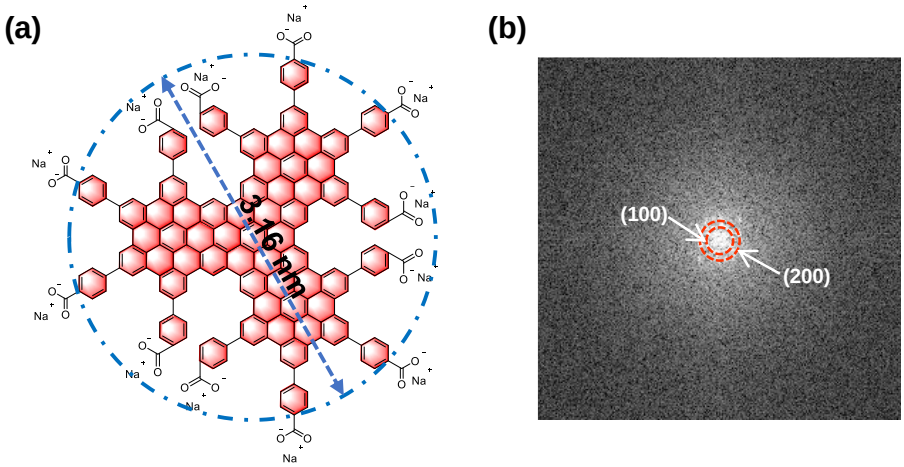

Figure S22. Theoretical diameter of HPGQD. (a)The internal core diameter of HPGQD is 3.16 nm according to the molecular structure. (b) The FFT profiles of HRTEM of HPGQD correspond to typical graphite (100) and (200) crystal planes.

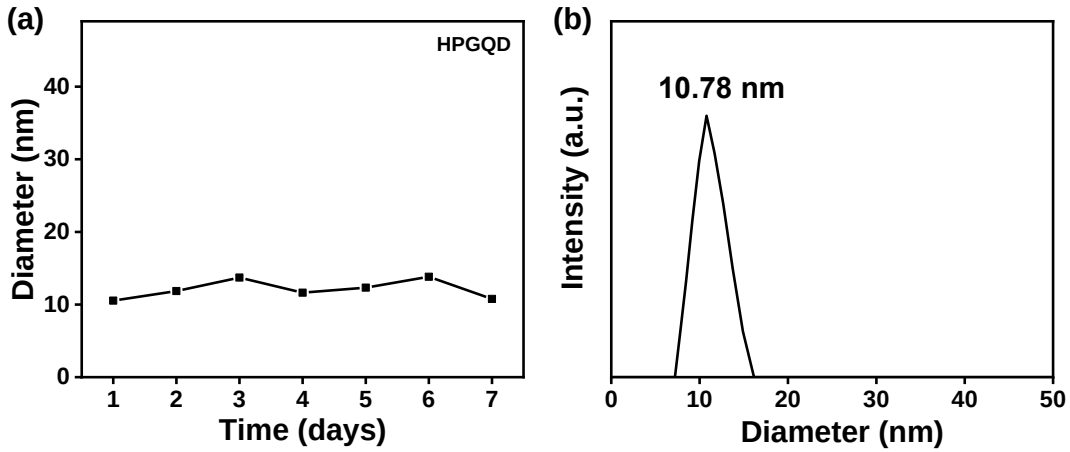

Figure S23. DLS Test**.** (a) the size changes of HPGQD in PBS containing HSA by time, measured by DLS. (b) DLS analysis of HPGQD in PBS (pH=7.4) on the seventh day. The PBS containing HSA for HPGQD (20 μmol L^{-1}) was sonicated for 0.5 h, filtered through a 0.22 μm microporous filter membrane, and the HPGQD particle size was measured using DLS.

Tabel S1. Particle size, PDI and zeta potential of HPGQD on the seventh day.

Samples	Size (nm)	PDI	Zeta (mV)
HPGQD	10.8 ± 0.2	0.016 ± 0.002	-23 ± 1

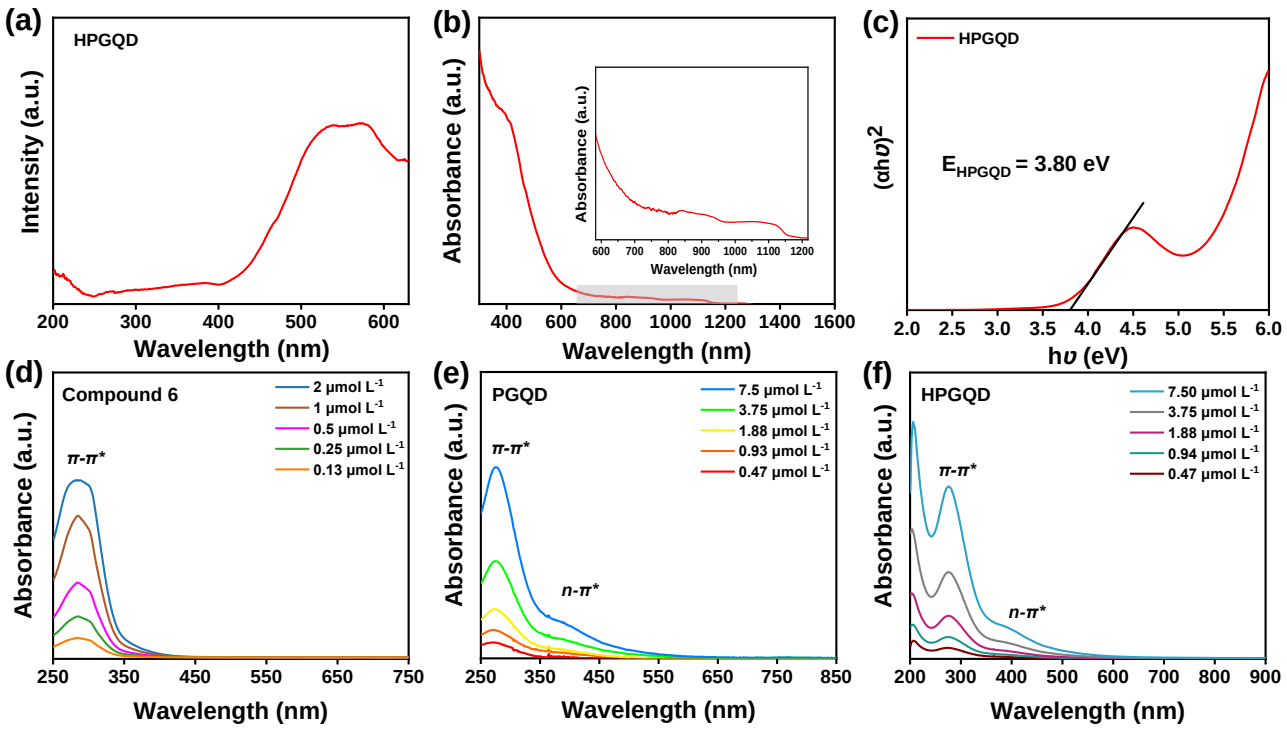

Figure S24. PL excitation spectrum and UV-Vis absorption spectrum. (a) PL excitation spectrum of HPGQD. (b) UV-Vis absorption spectrum of HPGQD (400-1600 nm). (c) Plot of $(\alpha h\nu)^2$ vs. $h\nu$ for HPGQD. (d) UV-Vis absorption spectrum of different concentration of Compound 6. (e) UV-Vis absorption spectrum of different concentration of PGQD (in DCM). (f) UV-Vis absorption spectrum of different concentration of HPGQD (in H_2O).

The Tauc Plot method was utilized to calculate the optical band gap from the UV-Vis absorption data[1]. The optical bandgap (E_g) is given by the intercept of a linear fit of the curve to the energy ($h\nu$) axis, shown in Figure S24C. The optical bandgap of HPGQD was obtained from the fitting to be 3.80 eV. The Tauc Plot relation used to calculate the optical bandgap is given by

$$h\nu = h\frac{c}{\lambda} \quad (1)$$

$$\alpha h\nu^{1/m} = B(h\nu - E_g) \quad (2)$$

where α, $h\nu$, m, B, and E_g denote the absorption coefficient, photon energy, empirical constant, constant, and optical bandgap, respectively. Where, α is obtained from UV-Vis absorption spectroscopy measurements. It is assumed that HPGQD is a direct bandgap material and the value of m is 1/2.

Tabel S2. Kinetic parameters for the PL decay curve fitting of HPGQD[2].

Sub	B_0	B_1	τ_1 (ns)	R_1	B_2	τ_2 (ns)	R_2	R^2	τ_{ave} (ns)
PGQD	7.991	1180.582	1.125	0.193	878.335	6.313	0.807	0.997	5.310
HPGQD	12.344	1317.182	1.213	0.171	999.493	7.766	0.829	0.997	6.647

The double exponential decay curve is fitted as shown as followed

$$\mathbf{R(t)=B_0+B_1e^{(-t/\tau_1)}+B_2e^{(-t/\tau_2)}} \quad \mathbf{(3)}$$

where B_0 stands for a constant, B_1 and B_2 stand for fractional intensities; $R(t)$ is the fluorescence intensity at time t; τ_1 and τ_2 are decay times; and t is time. The average fluorescence lifetime was calculated from the following formula

$$\boldsymbol{\tau_{ave}=\frac{B_1\tau_1^2+B_2\tau_2^2}{B_1\tau_1+B_2\tau_2}} \quad \mathbf{(4)}$$

$$\boldsymbol{\tau_1R_1+\tau_2R_2=\tau_{ave}} \quad \mathbf{(5)}$$

$$\mathbf{R_1+R_2=1} \quad \mathbf{(6)}$$

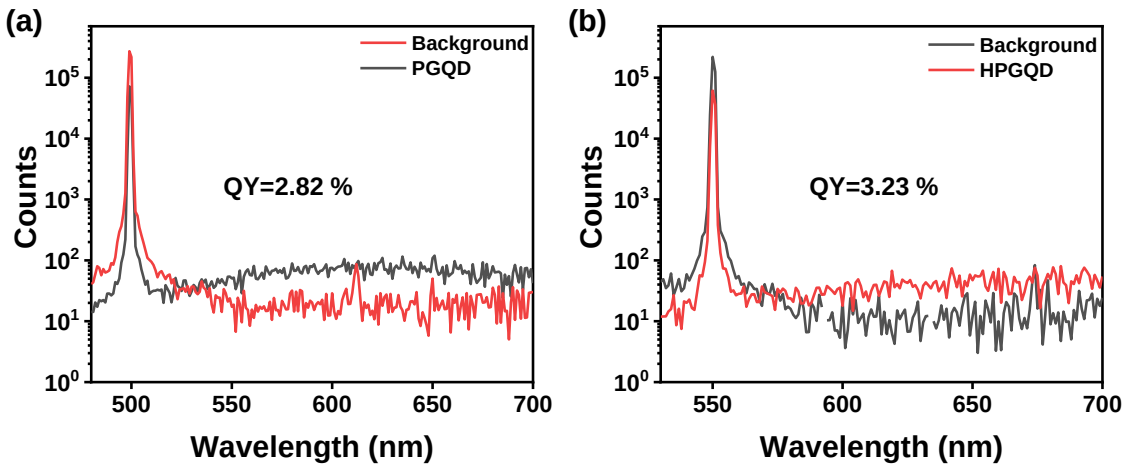

Figure S25. The PLQY of PGQD and HPGQD. (a) The PLQY of PGQD (in CH_2Cl_2) was measured to be 2.82 %, by absolute method using an integrating sphere. (b) The PLQY of HPGQD (in H_2O) was measured to be 3.23 %, by absolute method using an integrating sphere.

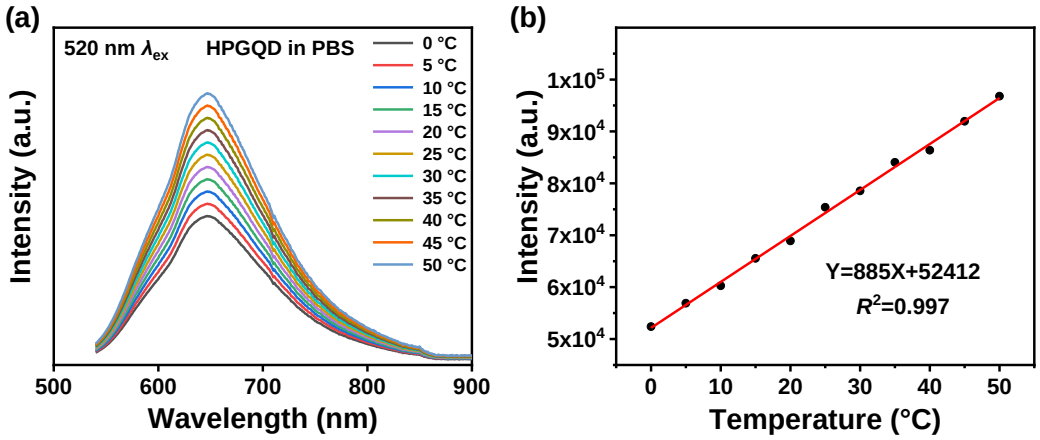

Figure S26. Fluorescence spectra of HPGQD in PBS at different temperatures. (a)The fluorescence stability of HPGQD (20 μmol L^{-1}) in PBS (pH=7.4) under different temperature (0-50 °C). (b) The linear fitting curve is based on the fluorescence intensity of HPGQD at different temperatures in Figure S26a.

Tabel S3. Complete functional group information for FTIR spectrum of PAH (Compound 6), PGQD and HPGQD.

Wavenumber (cm^{-1})	Functional groups	Vibration
3029	Ar-H	Stretching Vibration
2946	C-H ($-CH_3$)	Stretching Vibration
1718	C=O	Stretching Vibration
1602/1491	C=C	Stretching Vibration
1542/1398	COO^-	Stretching Vibration
1437	C-H	Bending Vibration
1280	C=C	Stretching Vibration
1190	C-H ($-CH_3$)	Bending Vibration
1109	C-O	Bending Vibration
1047	C-O	Stretching Vibration
833	Ar-H	Bending Vibration
762	Ar-H	Bending Vibration
698	Ar-H	Bending Vibration

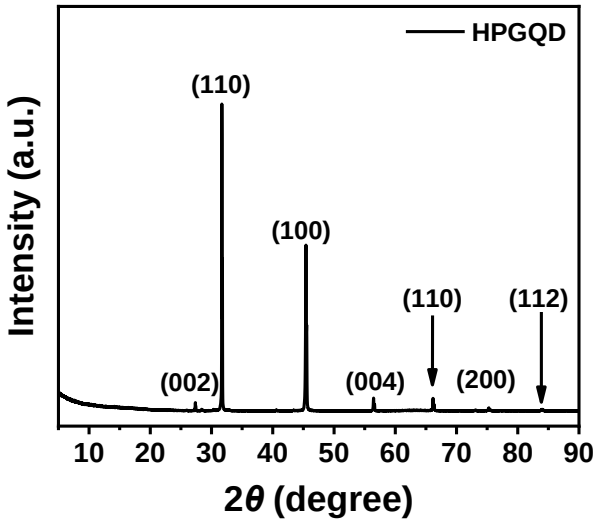

Figure S27. XRD pattern of HPGQD.

Table S4. The XRD Diffraction angles 2θ of HPGQD.

HPGQD		
Hkl	**2θ (°)**	***d* (Å)**
002	27.34	3.26
110	31.67	2.82
100	45.42	2.00
004	56.46	1.63
110	66.15	1.41
200	75.29	2.50 (n=2)
112	83.98	1.15

The specific steps for calculating the lattice spacing are as follows:

Determine the angle θ between the incident and diffracted rays by an X-ray diffraction experiment. Calculate the lattice spacing in the crystal from the Bragg diffraction equation：

$$2d \sin\theta = n\lambda \quad (7)$$

where d is the crystal plane spacing, θ is the angle between the incident ray and the crystal plane, λ: X-ray wavelength (1.5406 Å, Cu-Kα1), and n: positive integer (usually taken to be 1, which represents first-degree diffraction). With θ and λ known, the value of d, the crystal plane spacing, can be solved for.

Biological details.

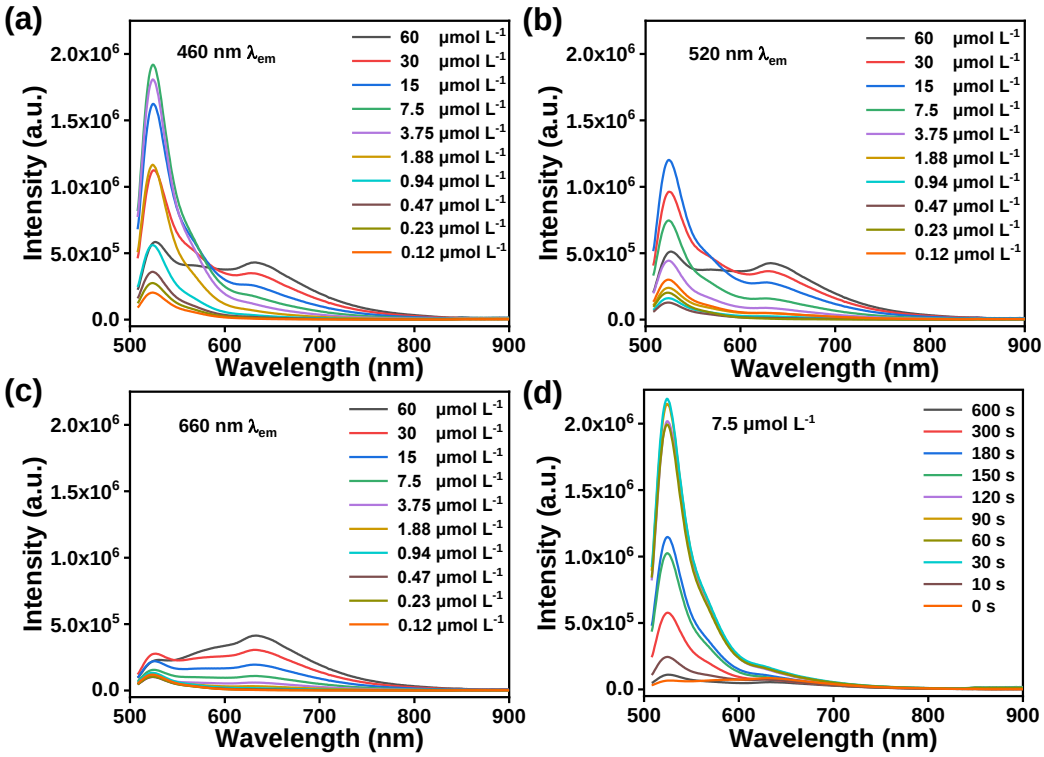

Figure S28. The impact of HPGQD concentration, irradiation time, and irradiation wavelength on ROS generation. (a) The ROS generation of HPGQD with different concentrations under 460 nm (20 mW cm^{-2}) irradiation for 30 s. (b) The ROS generation of HPGQD with different concentrations under 520 nm (20 mW cm^{-2}) irradiation for 30 s. (c) The ROS generation of HPGQD with different concentrations under 660 nm (20 mW cm^{-2}) irradiation for 30 s. (d) The ROS generation of HPGQD (7.5 μmol L^{-1}) with different irradiation times under 460 nm (20 mW cm^{-2}) irradiation.

Tabel S5. ESR spectroscopy to detect absolute quantitative program data for HPGQD.

Name	The spin concentration per unit volume (spins mm^{-3})	The molar concentration of the number of spins and electrons (mol L^{-1})	The total spin number (spins)
HPGQD	1.198×10^{11}	1.989×10^{-07}	3.763×10^{12}

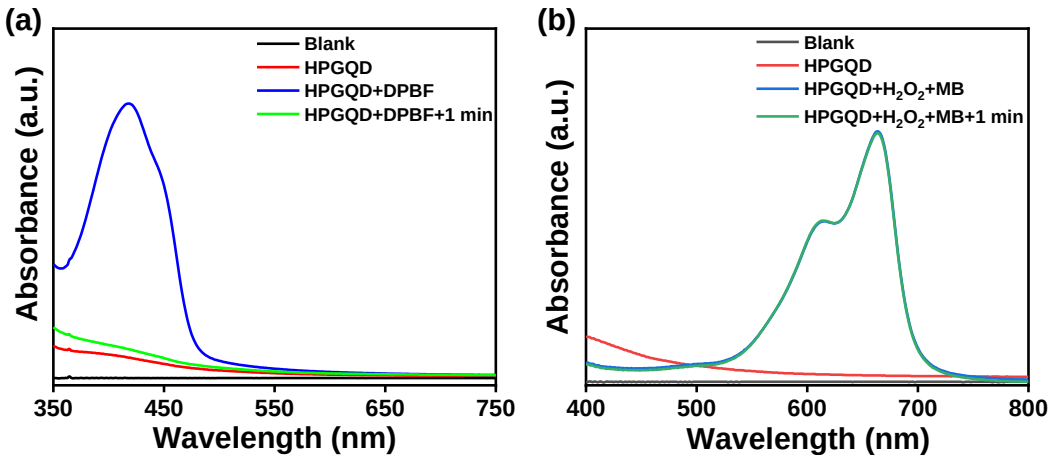

Figure S29. DPBF and MB are used to detect the types of ROS. (a) DPBF (0.25 mg mL^{-1}, 200 μL) and HPGQD (0.83 μmol L^{-1}, 3 mL), the $^1O_2$ generating capacity was observed by irradiation at 460 nm (20 mW cm^{-2}) for 1 min. (b) MB (300 μmol L^{-1}, 1 mL), H_2O_2 (3 mmol mL^{-1}, 1 mL) and HPGQD (0.83 μmol L^{-1}, 1 mL), the ·OH generating capacity was observed by irradiation at 460 nm (20 mW cm^{-2}) for 1 min.

Tabel S6. The $^1O_2$ quantum yield of previous studies.

Number	Materials	$^1O_2$ quantum yield	Reference
1	**HPGQD**	**0.85**	**This work**
2	C222 (1d)	0.67	[3]
3	MB	0.52	[4]
4	Eosin Y	0.6	[3]
5	Eosin B	0.37	[3]
6	5,10,15,20-tetrakis(4sulfonatophenyl)-21,23H-porphine ($H2TPPS^{4-}$)	0.6	[3]
7	RB	0.75	[5]
8	porous Si nanoparticles (PSiNP)	0.17	[6]
9	Mn-CD	0.4	[7]
10	PSDalpha	0.12	[8]
11	CdTe QDs	0.43	[9]
12	rGO-Ru-PEG	0.31	[10]
13	silicon nanorod (SiNR)	0.24	[11]

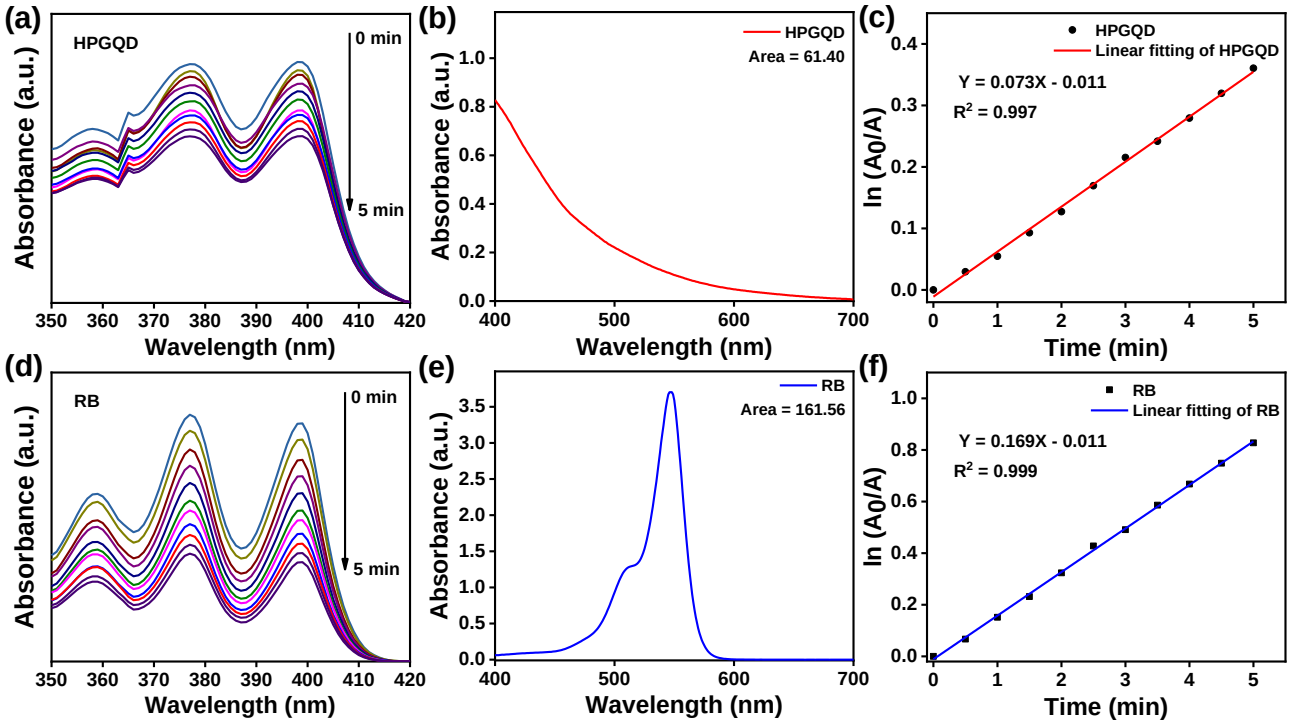

Figure S30. The measurements of the $^1O_2$ quantum yield of HPGQD[12]. (a) Photodegradation of Na_2-ADPA with HPGQD. (b) The absorption peak area of HPGQD. (c) The decomposition rate constants of Na_2-ADPA by HPGQD. (d) Photodegradation of Na_2-ADPA with RB. (e) The absorption peak area of RB. (f) The decomposition rate constants of Na_2-ADPA by RB.

The $^1O_2$ quantum yields of HPGQD in water were calculated using the following equation (8):

$$\Phi_{HPGQD} = \frac{\Phi_{RB} \times K_{HPGQD} \times A_{RB}}{K_{RB} \times A_{HPGQD}} \quad (8)$$

where K_{HPGQD} and K_{RB} are the rate constants for the decomposition of Na_2-ADPA by HPGQD and RB, respectively. A_{HPGQD} and A_{RB} represent the light absorbed by HPGQD and RB, respectively, which are determined by integrating over the light absorption bands in the wavelength range of 400-700 nm. Φ_{RB} is the $^1O_2$ quantum yield of RB, which is 0.75 in water.

In Figure S28, the decomposition rate constants K_{HPGQD} and K_{RB} can be determined to be 0.073 and 0.169, respectively. (Figure S28c, S28f). In addition, A_{HPGQD} is 61.40 (Figure S28b) and A_{RB} is 161.56 (Figure S28e). Thus, substituting Φ_{RB} (0.75) into the equation (1). Eventually, Φ_{HPGQD} can be calculated to be 0.85 ($^1O_2$ quantum yield of HPGQD in water).

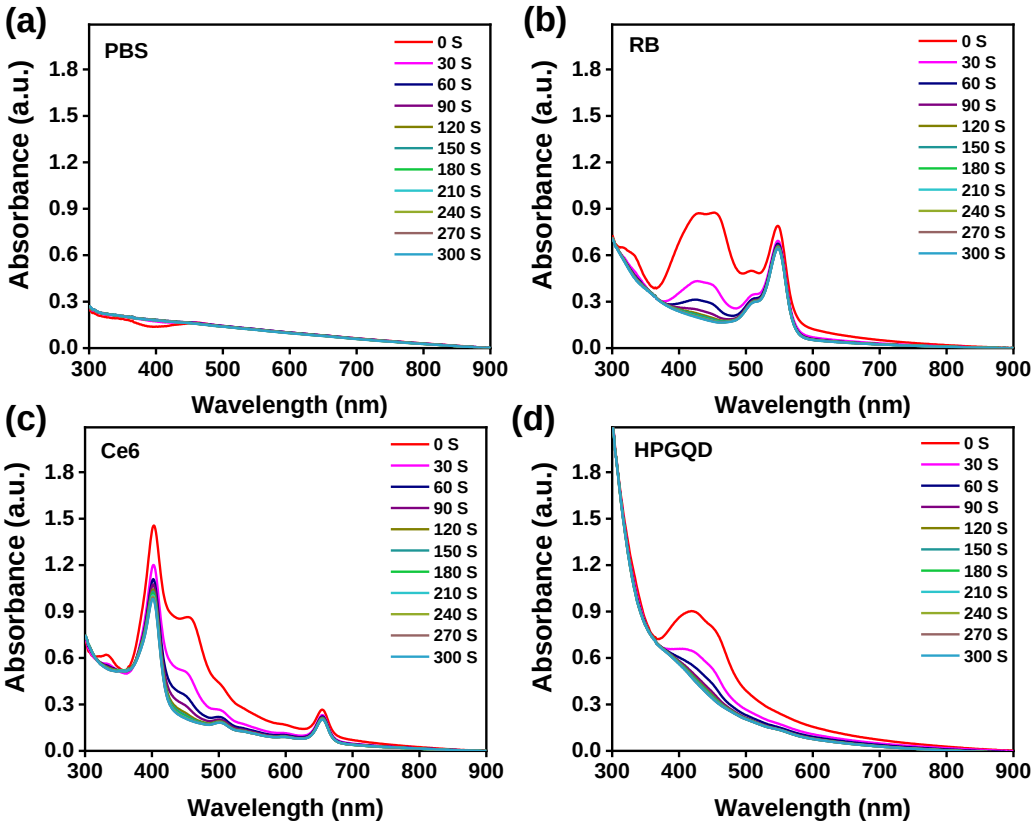

Figure S31. The ROS generation ability of type Ⅱ photosensitizers. Type-II ROS generation capability evaluation of HPGQD, Ce6, and RB with DPBF (100 μmol L^{-1}, 5 μL) as the indicator. All concentrations are 7.5 μmol L^{-1}, 460 nm (20 mW cm^{-2}).

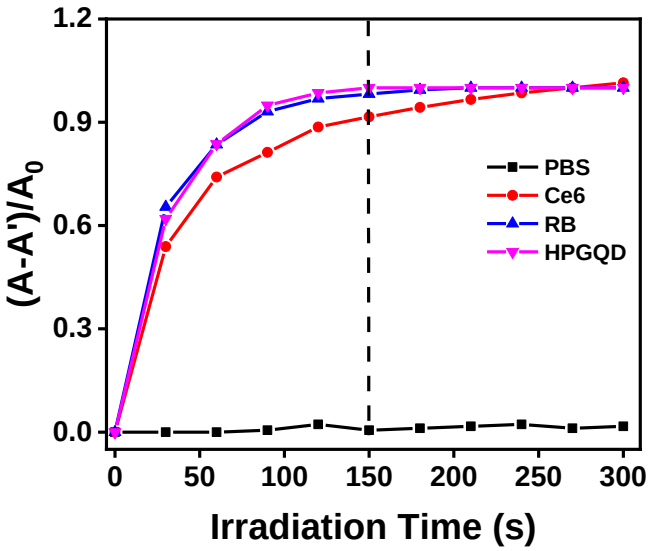

Figure S32. The ROS generation ability of type Ⅱ photosensitizers. HPGQD, Ce6 and RB use DPBF (100 μmol L^{-1}, 5 μL) as an indicator to compare the absorption intensity at 410 nm (460 nm, 20 mW cm^{-2}).

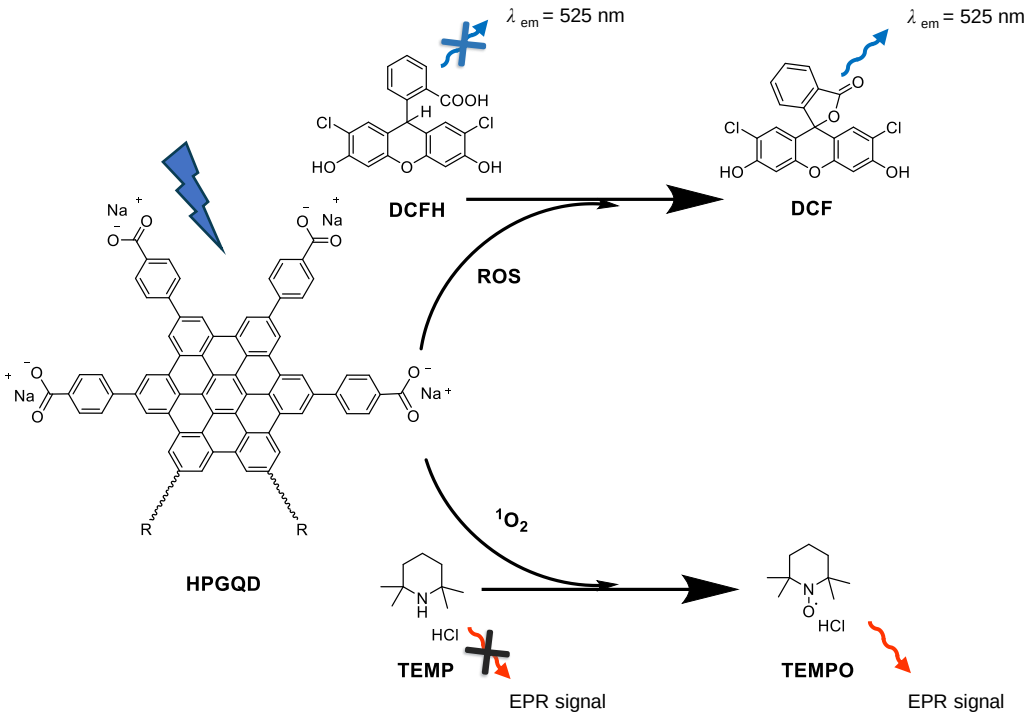

Figure S33. FL and ESR methods to verify the type of ROS generated by HPGQD. Chemical structure of DCFH and the formation of DCF upon interaction with ROS lead to the activation of FL output; Chemical structure of TEMP and the formation of the stabilized nitrogen-oxygen radical TEMPO upon interaction with $^1O_2$.

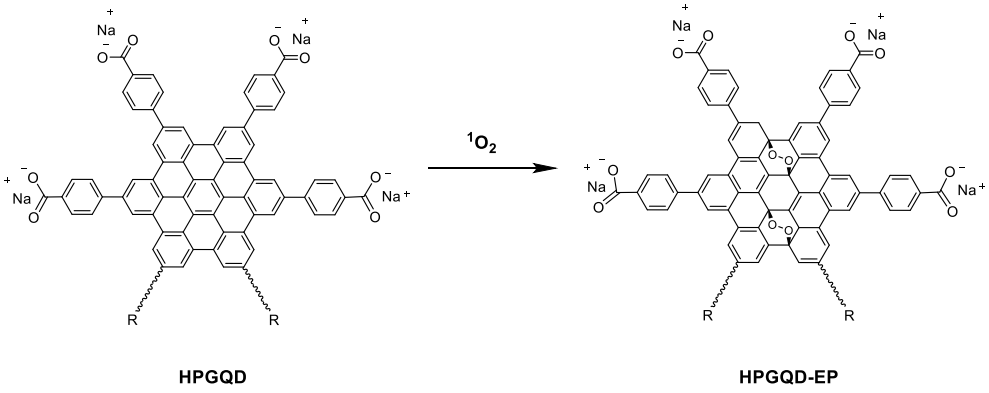

Figure S34. Mechanism of HPGQD scavenging $^1O_2$. Schematic of the chemical structure of HPGQD and the formation of HPGQD-EP upon interaction with $^1O_2$, leading to a dramatic decrease in the production of $^1O_2$.

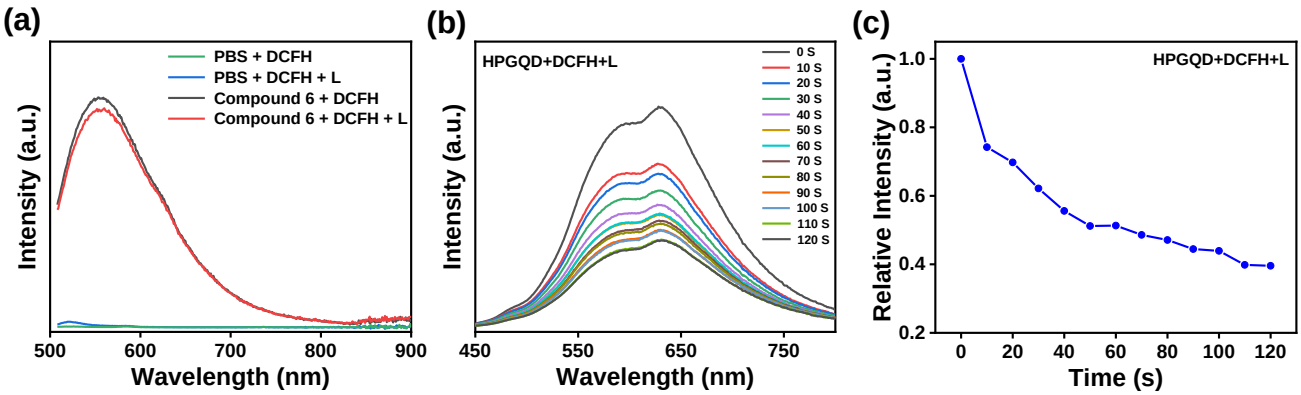

Figure S35. Mechanism of HPGQD scavenging $^1O_2$. (a) PAH (Compound 6) (7.5 μmol L^{-1}) does not produce ROS under irradiation for 3 min. (b) After HPGQD+DCFH with irradiation, the FL output of continuous irradiation decreased. The formation of HPGQD-EP results in the change of the carbon sp^2 conjugate structure in the core plane of HPGQD (7.5 μmol L^{-1}), 460 nm (20 mW cm^{-2}). (c) Quantitative analysis of fluorescence intensity with irradiation time based on Fig S34b.

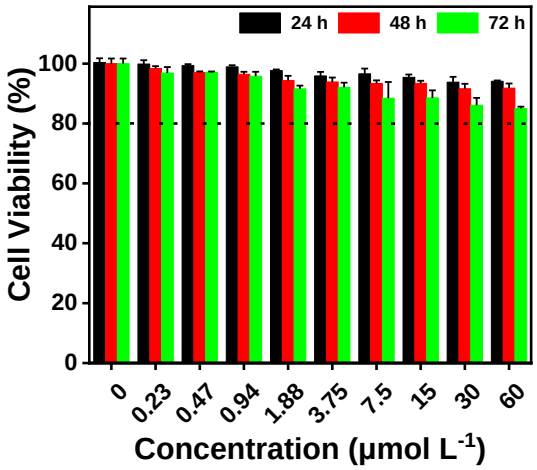

Figure S36. Dark cytotoxicity of HPGQD. 4T1 cells viability was assessed by MTT assay after co-incubated with different concentrations of HPGQD for 24, 48 and 72 h. All data are expressed as mean ± SD (n = 5).

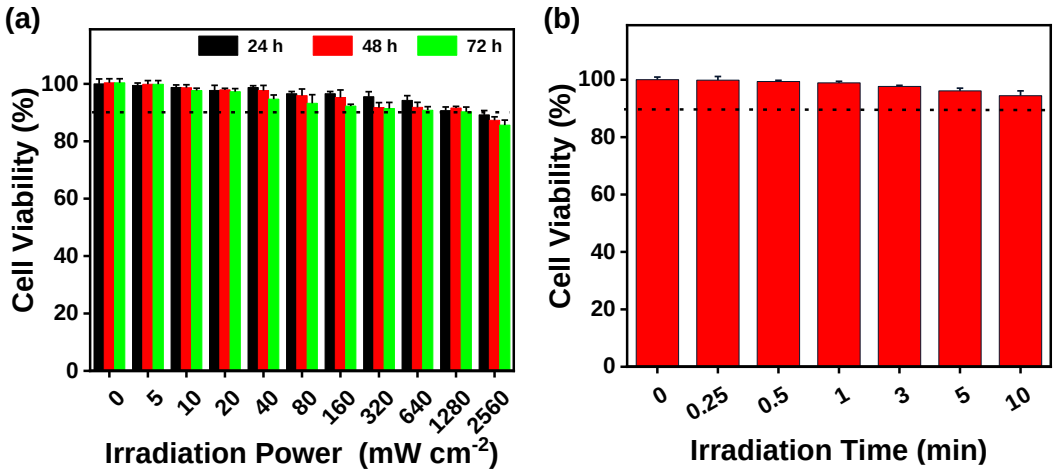

Figure S37. Dark cytotoxicity of 4T1 cells under different laser power and irradiation time. (a) under different laser power (460 nm, 30 s), after incubation for 24, 48 and 72 h, 4T1 cells viability was assessed by MTT assay. (b) under different laser irradiation time (460 nm, 1.5 W cm^{-2}), 4T1 cells viability was assessed by MTT assay after incubation for 72 h. All data are expressed as mean ± SD (n = 5).

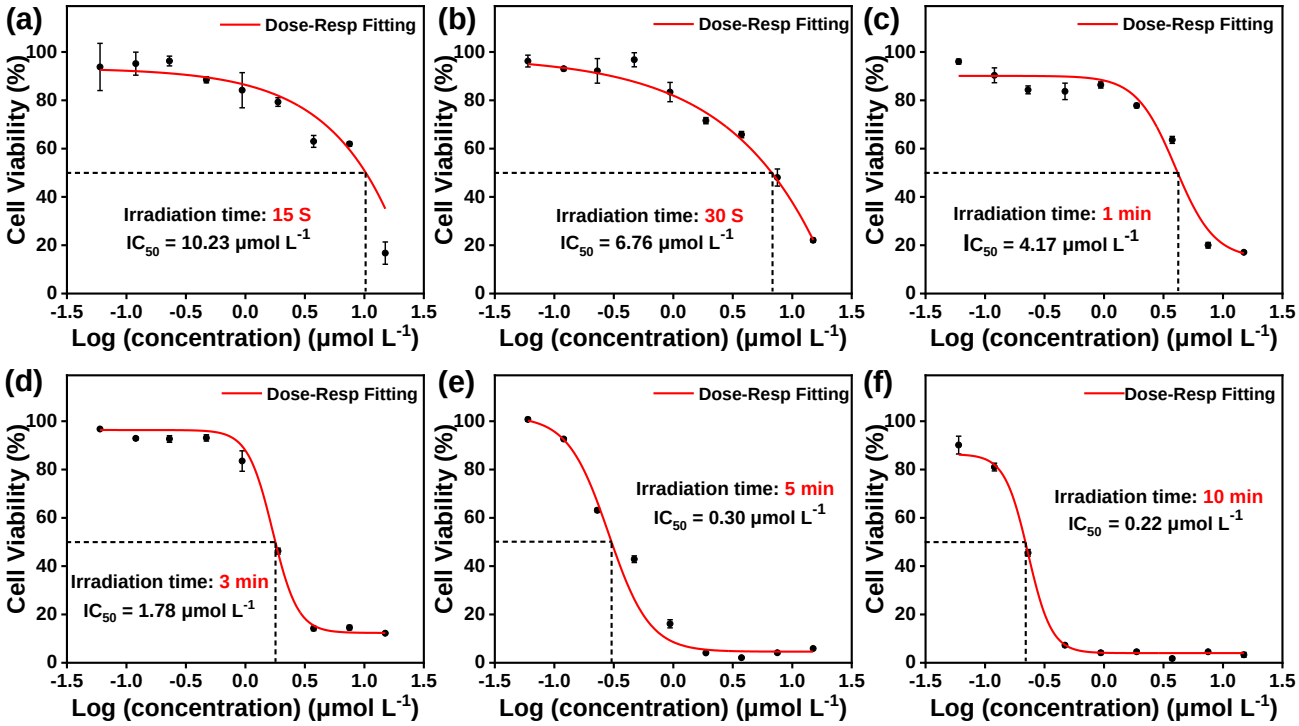

Figure S38. IC_{50} values under different irradiation times were obtained through Dose-Response curves fitting[13]. (a-f) The concentrations were 0.06, 0.12, 0.23, 0.47, 0.94, 1.88, 3.75, 7.5, and 15 μmol L^{-1} (The horizontal coordinate is the logarithmic value of the concentration, and the vertical coordinate is the cell viability).

Tabel S7. IC_{50} values for different irradiation times of HPGQD.

Number	Irradiation time (min)	IC_{50} value (μmol L^{-1})
1	0.25	10.23
2	0.5	6.76
3	1	4.17
4	3	1.78
5	5	0.30
6	10	0.22

Tabel S8. IC_{50} of different carbon-based nanomaterials used for PDT with irradiation concentration and time.

Number	Carbon-based nanomaterials	Concentration ($\mu g\ mL^{-1}$)	Irradiation time (min)	Reference
1	**HPGQD**	**5.89 (1.78 µmol L^{-1})**	**3**	**This work**
2	GQD particles	~ 200	10	[14]
3	Cu(II)Chl-HA NPs	~ 75	5	[15]
4	Cu-CD	~ 250	12	[16]
5	γ-PGA@Gox @Mn,Cu-CDs NPs	~ 40	10	[17]
6	CDs	~ 25	10	[18]
7	C225-PNDs	~ 10	30	[19]
8	MnPCNDs	~ 20	30	[20]
9	UCNP-GQD/TRITC	~ 80	5	[21]
10	GQD@MnO_2	~ 20	30	[22]
11	N-GQD-DOX-APTES	~ 5	20	[23]
12	PC@GCpD(Gd)	~ 30	10	[24]

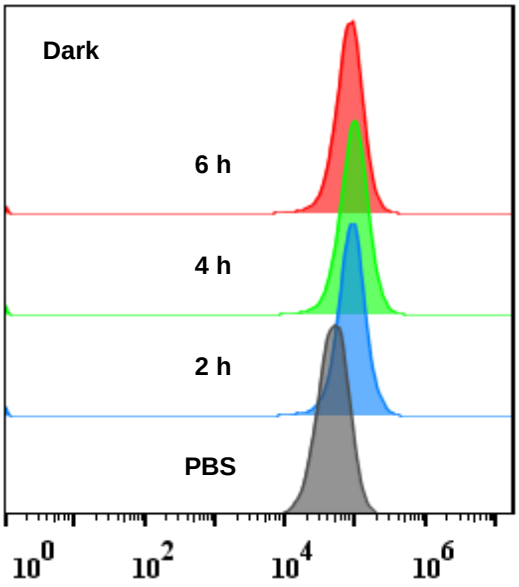

Figure S39. ROS generation of 4T1 cells co-incubated with HPGQD (3 μmol L^{-1}) for 2, 4 and 6 h by DCFH-DA without irradiation.

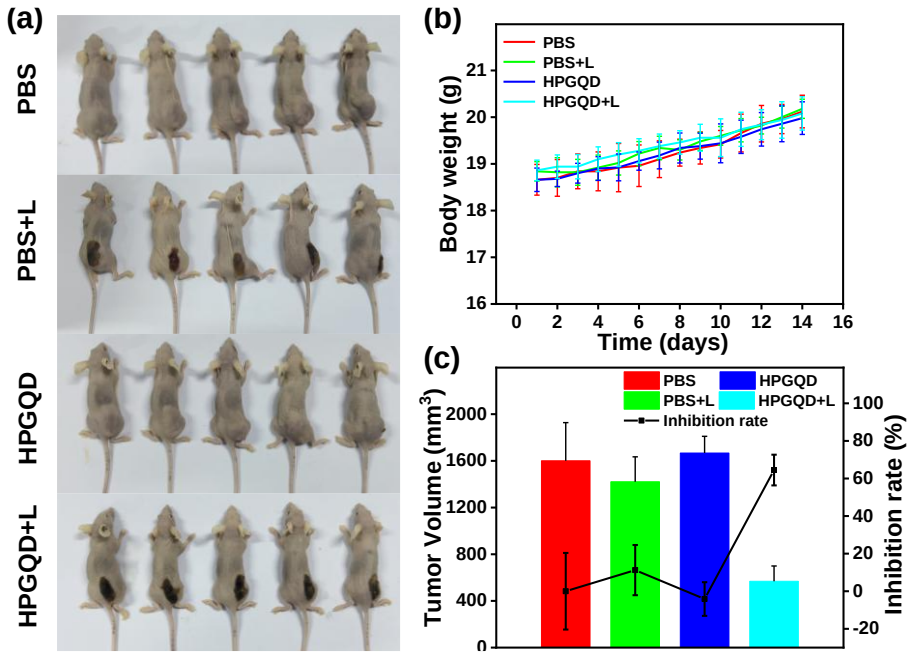

Figure S40. (a) Pre-dissection photographs of mice treated for 14 days. (b) The changes in body weight of mice treated for 14 days. (c) Quantitative analysis of tumor volumes on the 14th day after PDT treatment. Data are presented as mean ± SD (n = 5).

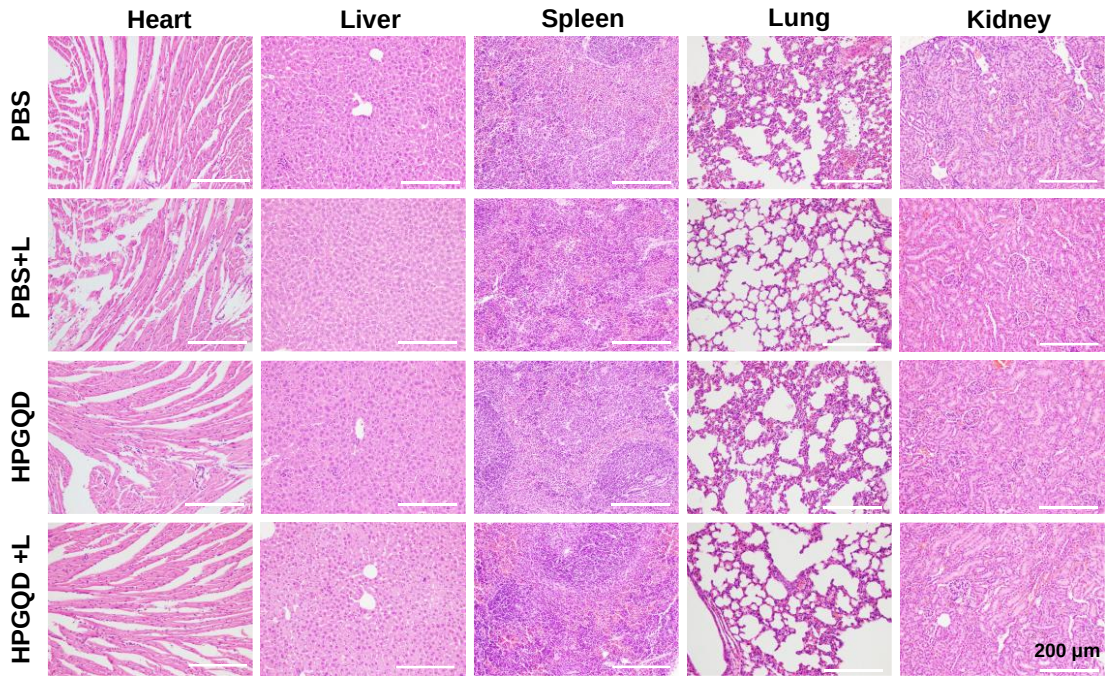

Figure S41. H&E staining images of critical organs (heart, liver, spleen, Lung, and kidney) of PBS, PBS+L, HPGQD and HPGQD+L groups. (Scale bar: 200 μm).

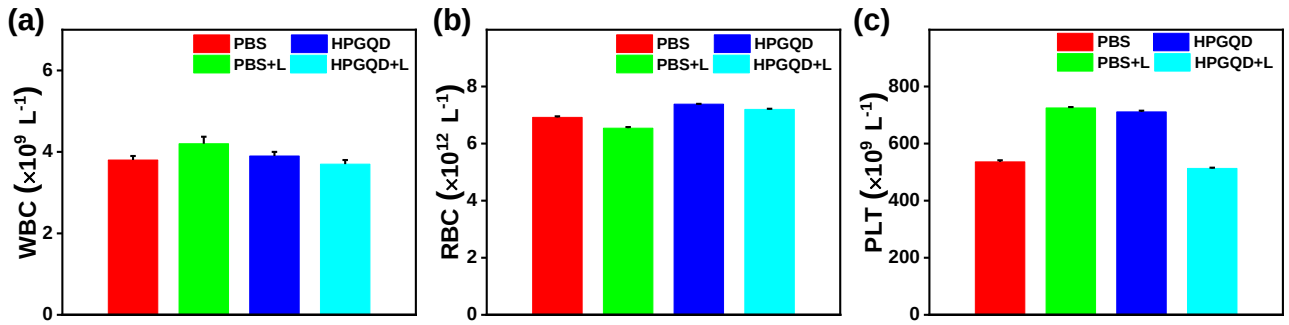

Figure S42. (a-c) The whole blood cell analysis (WBC, RBC, PLT) of PBS, PBS+L, HPGQD and HPGQD +L groups. All data are presented as mean ± SD (n = 3).

Tabel S9. Mean values of whole blood cytometric analysis for PBS, PBS+L, HPGQD and HPGQD +L groups (n = 3).

Testing Programs	PBS	PBS+L	HPGQD	HPGQD+L	Reference Range
WBC ($\times10^9$ L^{-1})	3.8	4.2	3.9	3.7	0.8-6.8
RBC ($\times10^{12}$ L^{-1})	6.92	6.54	7.38	7.20	6.36-9.42
PLT ($\times10^9$ L^{-1})	536	725	711	513	450-1590

Tabel S10. Correspondence table between abbreviations and full Name.

Number	Abbreviations	Full Name
1	GQDs	Graphene Quantum Dots
2	PAH	Polycyclic Aromatic Hydrocarbons
3	NMR	Nuclear Magnetic Resonance
4	FTIR	Fourier Transform Infrared Spectroscopy
5	TLC	Thin-Layer Chromatography
6	TEM	Transmission Electron Microscopy
7	HRTEM	High-Resolution Transmission Electron Microscopy
8	AFM	Atomic Force Microscopy
9	OD	optical density
10	MALDI	Matrix-Assisted Laser Desorption/Ionization
11	TOF-MS	Time-of-Flight- Mass Spectroscopy
12	DLS	Dynamic Light Scattering
13	FL	Fluorescence
14	PL	Photoluminescence
15	QY	Quantum Yield
16	DCFH-DA	2',7'-Dichlorodihydrofluorescein Diacetate
17	DCF	2',7'-Dichlorofluorescein
18	4T1 cells	Mouse breast cancer (4T1) cells
19	MTT	3-(4, 5-dimethylthiazol-2-yl)-2, 5-diphenyl tetrazolium bromide
20	CLSM	Confocal Laser Scanning Microscopy
21	FCM	Flow Cytometry Microscopy
22	HE	Hematoxylin and Eosin
23	TUNEL	Terminal Deoxynucleotidyl Transferase dUTP Nick End Labeling
24	DCM	Dichloromethane
25	Ph_2O	Phenyl Ether
26	THF	Tetrahydrofuran
27	MeOH	Methanol
28	ROS	Reactive Oxygen Species

References

1 A. N. Nair, V. S. N. Chava, S. Bose, T. Zheng, S. Pilla and S. T. Sreenivasan, In Situ Doping-Enabled Metal and Nonmetal Codoping in Graphene Quantum Dots: Synthesis and Application for Contaminant Sensing, *ACS Sustainable Chem. Eng.*, 2020, **8**, 16565-16576.

2 M. Park, Y. Jeong, H. S. Kim, W. Lee, S. H. Nam, S. Lee, H. Yoon, J. Kim, S. Yoo and S. Jeon, Quenching-Resistant Solid-State Photoluminescence of Graphene Quantum Dots: Reduction of π–π Stacking by Surface Functionalization with POSS, PEG, and HDA, *Adv. Funct. Mater.*, 2021, **31**, 2102741.

3 X.-H. Ma, X. Gao, J.-Y. Chen, M. Cao, Q. Dai, Z.-K. Jia, Y.-B. Zhou, X.-J. Zhao, C. Chu, G. Liu and Y.-Z. Tan, Soluble Nanographene C222: Synthesis and Applications for Synergistic Photodynamic/Photothermal Therapy, *J. Am. Chem. Soc.*, 2024, **146**, 2411-2418.

4 S. S. Khatoon, Y. Chen, H. Zhao, F. Lv, L. Liu and S. Wang, In situ self-assembly of conjugated polyelectrolytes for cancer targeted imaging and photodynamic therapy, *Biomater. Sci.*, 2020, **8**, 2156-2163.

5 R. W. Redmond and J. N. Gamlin, A Compilation of Singlet Oxygen Yields from Biologically Relevant Molecules, *Photochem. Photobiol.*, 2008, **70**, 391-475.

6 L. Xiao, L. Gu, S. B. Howell and M. J. Sailor, Porous Silicon Nanoparticle Photosensitizers for Singlet Oxygen and Their Phototoxicity against Cancer Cells, *ACS Nano*, 2011, **5**, 3651–3659.

7 Q. Jia, J. Ge, W. Liu, X. Zheng, S. Chen, Y. Wen, H. Zhang and P. Wang, A Magnetofluorescent Carbon Dot Assembly as an Acidic H2O2-Driven Oxygenerator to Regulate Tumor Hypoxia for Simultaneous Bimodal Imaging and Enhanced Photodynamic Therapy, *Adv. Mater.*, 2018, **30**, e1706090.

8 S. Zhang, Y. Li, T. Li, Y. Zhang, H. Li, Z. Cheng, N. Peng, Y. Liu, J. Xu and H. He, Activable Targeted Protein Degradation Platform Based on Light-triggered Singlet Oxygen, *J. Med. Chem.*, 2022, **65**, 3632-3643.

9 L. Shi, B. Hernandez and M. Selke, Singlet oxygen generation from water-soluble quantum dot–organic dye nanocomposites, *J. Am. Chem. Soc.*, 2006, **128**, 6278-6279.

10 D.-Y. Zhang, Y. Zheng, C.-P. Tan, J.-H. Sun, W. Zhang, L.-N. Ji and Z.-W. Mao, Graphene Oxide Decorated with Ru(II)–Polyethylene Glycol Complex for Lysosome-Targeted Imaging and Photodynamic/Photothermal Therapy, *ACS Appl. Mater. Interfaces*, 2017, **9**, 6761-6771.

11 Q. Jia, M. Chen, Q. Liu, W. Liu, H. Zhang, J. Ge and P. Wang, Ethylene glycol-mediated synthetic route for production of luminescent silicon nanorod as photodynamic therapy agent, *Sci. China Mater.*, 2017, **60**, 881-891.

12 J. Ge, M. Lan, B. Zhou, W. Liu, L. Guo, H. Wang, Q. Jia, G. Niu, X. Huang, H. Zhou, X. Meng, P. Wang, C.-S. Lee, W. Zhang and X. Han, A graphene quantum dot photodynamic therapy agent with high singlet oxygen generation, *Nat. Commun.*, 2014, **5**, 4596.

13 Z. Li, D. Wang, M. Xu, J. Wang, X. Hu, S. Anwar, A. C. Tedesco, P. C. Morais and H. Bi, Fluorine-containing graphene quantum dots with a high singlet oxygen generation applied for photodynamic therapy, *Journal of Materials Chemistry B*, 2020, **8**, 2598-2606.

14 Z. M. Markovic, B. Z. Ristic, K. M. Arsikin, D. G. Klisic, L. M. Harhaji-Trajkovic, B. M. Todorovic-Markovic, D. P. Kepic, T. K. Kravic-Stevovic, S. P. Jovanovic, M. M. Milenkovic, D. D. Milivojevic, V. Z. Bumbasirevic, M. D. Dramicanin and V. S. Trajkovic, Graphene quantum dots as autophagy-inducing photodynamic agents, *Biomaterials*, 2012, **33**, 7084-7092.

15 Z. Guo, X. Zhou, C. Hou, Z. Ding, C. Wen, L.-J. Zhang, B.-P. Jiang and X.-C. Shen, A chloroplast-inspired nanoplatform for targeting cancer and synergistic photodynamic/photothermal therapy, *Biomater. Sci.*, 2019, **7**, 3886-3897.

16 J. Wang, M. Xu, D. Wang, Z. Li, F. L. Primo, A. C. Tedesco and H. Bi, Copper-Doped Carbon Dots for Optical Bioimaging and Photodynamic Therapy, *Inorg. Chem.*, 2019, **58**, 13394-13402.

17 M. Zhang, W. Wang, F. Wu, T. Zheng, J. Ashley, M. Mohammadniaei, Q. Zhang, M. Wang, L. Li, J.

Shen and Y. Sun, Biodegradable Poly(γ-glutamic acid)@glucose oxidase@carbon dot nanoparticles for simultaneous multimodal imaging and synergetic cancer therapy, *Biomaterials*, 2020, **252**, 120106.
18 S. Zhao, S. Wu, Q. Jia, L. Huang, M. Lan, P. Wang and W. Zhang, Lysosome-targetable carbon dots for highly efficient photothermal/photodynamic synergistic cancer therapy and photoacoustic/two-photon excited fluorescence imaging, *Chem. Eng. J.*, 2020, **388**, 124212.
19 F. Wu, H. Su, Y. Cai, W.-K. Wong, W. Jiang and X. Zhu, Porphyrin-Implanted Carbon Nanodots for Photoacoustic Imaging and in Vivo Breast Cancer Ablation, *ACS Appl. Bio Mater.*, 2018, **1**, 110-117.
20 F. Wu, J. Chen, Z. Li, H. Su, K. C.-F. Leung, H. Wang and X. Zhu, Red/Near-Infrared Emissive Metalloporphyrin-Based Nanodots for Magnetic Resonance Imaging-Guided Photodynamic Therapy In Vivo, *Part. Part. Syst. Charact.*, 2018, **35**, 1800208.
21 D. Zhang, L. Wen, R. Huang, H. Wang, X. Hu and D. Xing, Mitochondrial specific photodynamic therapy by rare-earth nanoparticles mediated near-infrared graphene quantum dots, *Biomaterials*, 2018, **153**, 14-26.
22 H.-M. Meng, D. Zhao, N. Li and J. Chang, A graphene quantum dot-based multifunctional two-photon nanoprobe for the detection and imaging of intracellular glutathione and enhanced photodynamic therapy, *The Analyst*, 2018, **143**, 4967-4973.
23 J. Ju, S. Regmi, A. Fu, S. Lim and Q. Liu, Graphene quantum dot based charge-reversal nanomaterial for nucleus-targeted drug delivery and efficiency controllable photodynamic therapy, *J. Biophotonics*, 2019, **12**, e201800367.
24 C. Wu, X. Guan, J. Xu, Y. Zhang, Q. Liu, Y. Tian, S. Li, X. Qin, H. Yang and Y. Liu, Highly efficient cascading synergy of cancer photo-immunotherapy enabled by engineered graphene quantum dots/photosensitizer/CpG oligonucleotides hybrid nanotheranostics, *Biomaterials*, 2019, **205**, 106-119.